Politecnico di Torino

MSc in Automotive Engineering
Academic Year 2025/2026

Formula Student Suspensions:

4-way damper characteristic and optimization setup

Supervisor:
Prof. Andrea Tonoli
Prof. Alessandro Vigliani
PhD Stefano Favelli

Candidate:
Alessandro Filippini

Abstract

The characteristic curves of passive hydraulic dampers represent a critical aspect of vehicle dynamics, as their setup requires a compromise between platform control, tyre-load variation and driveability. In motorsport applications, handling performance takes precedence, while comfort is considered mainly to the extent necessary to prevent excessive vibrations from affecting the driver's performance and visibility.
The aim of this work is to identify an effective baseline damper characteristic curve for the Formula Student prototype developed by the Squadra Corse PoliTo team, working within the adjustment range of the passive hydraulic dampers already installed on the vehicle and without modifying the existing suspension hardware.
A physics-based model of the car was first implemented in VI-CarRealTime vehicle dynamics software. Its results were compared with data acquired during on-track tests through a MATLAB/Simulink co-simulation framework in which real track inputs were fed to the virtual model. The correlation process focused on the model's ability to reproduce the main amplitudes and transient behaviour of the real prototype during double lane changes, steering-frequency sweeps and slalom manoeuvres. The comparison showed that the model reproduced the main measured trends and amplitudes with sufficient accuracy for the subsequent comparative analysis.
A set of freshly serviced four-way dampers was then tested by the team's external supplier, Lorandi Sospensioni, to obtain their force-velocity characteristic curves. Six nonlinear characteristics, resulting from discrete adjuster settings selected on the basis of the supplier's experience, were used to define the available tuning range. The different configurations were initially assessed using their wheel-side equivalent damping ratio at 20 mm/s and reduced-order quarter-car and roll models. The retained sets were then compared through a 43 s steering chirp and closed-loop virtual-driver simulations on the team's reference track, considering lap time, tyre loads, sideslip angle, driver-control activity and wheel lift.
The post-processing of the virtual hot laps highlighted some critical conditions during rapid lateral manoeuvres, mainly associated with the vehicle approaching its physical limits and temporarily losing road contact at specific wheels. Set 1 achieved the fastest lap, with a time of 39.520 s, while the configurations with the highest and lowest equivalent damping levels were approximately 3% slower. The least-damped configuration also required the greatest steering activity and produced sideslip-angle excursions exceeding 22° in absolute value. Wheel lift occurred predominantly at the inside rear wheel during combined braking and cornering, although the number of events alone was not sufficient to describe their severity.
Overall, the results indicate that an appropriate damper setup can reduce undesirable dynamic reactions, leading to more predictable vehicle behaviour and potentially improving overall performance. Within the investigated configurations, Set 5 provided the most favourable overall compromise. Its lap-time penalty relative to Set 1 was limited to 0.26 s (0.66%), while it produced a lower sideslip response, no front-wheel-lift events and a more favourable high-frequency contact-patch load response. Its larger cumulative wheel-lift duration remains a limitation. The result should therefore be considered as a baseline selection rather than a universal optimum and should be confirmed through controlled back-to-back track testing.

Table of Contents

Abstract **1**
1 Introduction **7**
1.1 Formula Student 7
1.2 Static Events 9
1.3 Dynamic Events 10
1.4 Competitive and Technical Context 11
1.5 SC24 Overview 13
1.6 Thesis Outline 14
1.7 Objectives 15
2 Theoretical Foundations **16**
2.1 Tyre Forces and Load Transfer 16
2.1.1 Tyre force generation and load sensitivity 16
2.1.2 Lateral load transfer and its distribution 17
2.1.3 Lateral response, roll and pitch transients 18
2.2 From Suspension Geometry to Wheel-Domain Properties 19
2.2.1 Double-wishbone push-rod architecture 19
2.2.2 Motion ratio, wheel rate and installed damping 20
2.2.3 Ride frequency, roll stiffness and coupled modes 21
2.3 Vertical Dynamics and Frequency-Domain Interpretation 21
2.3.1 Two-degree-of-freedom quarter-car model 21
2.3.2 Natural modes and damping ratio 22
2.3.3 Transmissibility, road holding and frequency response 23
2.4 Hydraulic Dampers and Nonlinear Force-Velocity Behaviour 24
2.4.1 Origin of the damping force and four-way adjustment 24
2.4.2 Quantifying nonlinear force-velocity curves 25
2.4.3 Compression-rebound asymmetry and vehicle-level implications 26
3 Formula Student Prototype and Virtual Vehicle Model **27**
3.1 Vehicle Overview and Suspension Architecture 27
3.2 Suspension Parameters and Damper Integration in the Virtual Model 28
3.3 Virtual Vehicle Model in VI-CarRealTime 30
3.4 MATLAB/Simulink Co-Simulation and Input Feeding 31
3.5 Track-Test Instrumentation 32
3.5.1 MicroAutoBox II 32
3.5.2 IMU - SBG Ellipse-N 32
3.5.3 Vehicle Sideslip-Angle Sensor - Kistler CORREVIT S-Motion Standard 33
3.5.4 Steering-Angle Sensor 34
3.6 On-Track Telemetry and Validation Manoeuvres 34
3.7 Model-to-Track Correlation and Discussion 35
3.7.1 Frequency Sweep 35
3.7.2 Double Lane Change 38
3.7.3 Slalom 40

3.8 Validation Comments 43
4 Experimental Characterisation of the Dampers 45
4.1 Damper Characterisation and Supplied Damper Data 45
4.2 Damper Hardware and Test Data Overview 45
4.3 Preliminary Screening Criterion 46
4.4 Selected Configurations 47
4.5 Reduced-Order Dynamic Assessment and Link to Damper Optimisation 49
4.5.1 Vertical Response 49
4.5.2 Roll Response 51
5 Damper Setup Tuning 54
5.1 Objectives and KPI Analysis 54
5.2 Simulation Setup and Evaluation Metrics 54
5.3 Standardised Steering Chirp Manoeuvre for Damper Setup Evaluation 55
5.3.1 Frequency Response Function 55
5.4 Comparison of Lap Time and Global Vehicle Behaviour 61
5.5 Wheel Load Management and Wheel Lift Analysis 68
6 Conclusions 71
Bibliography 74

List of Figures

Figure 1.1 Formula Student teams at an international event 7
Figure 1.2 Static and dynamic event categories in Formula Student (adapted from [1]) 9
Figure 1.3 SC24 Formula Student prototype 13
Figure 2.1 Schematic effect of tyre load sensitivity on the combined force capability of an axle. The curves are illustrative rather than tyre-specific; author's elaboration based on [2]. 17
Figure 2.2 First-order decomposition of lateral load transfer at one axle into the sprung-mass geometric, elastic and transient damping contributions and the unsprung-mass contribution; author's elaboration based on [2-4]. 18
Figure 2.3 Double-wishbone push-rod suspension model generated in VI-SuspensionGen (author's screenshot; software by VI-grade [14]) 20
Figure 2.4 Linear two-degree-of-freedom quarter-car model used to interpret ride and road-holding behaviour; adapted from [2,5]. 22
Figure 2.5 Displacement transmissibility of a base-excited single-degree-of-freedom system. All curves pass through $T_x = 1$ at $r = \sqrt{2}$; author's calculation from Equation (2.16), based on [5]. 23
Figure 2.6 Idealised linear, digressive and progressive force-velocity laws, together with an asymmetric digressive characteristic and its hydraulic operating regions; author's elaboration based on [6,8,11,12]. 25
Figure 3.1 SC24 front suspension model and hard-point layout 28
Figure 3.2 Öhlins TTX 25 MkII FSAE damper cutaway (source: Öhlins Racing public product documentation [18]) 29
Figure 3.3 Compression and rebound adjustment circuits of the Öhlins TTX 25 MkII FSAE damper (source: Öhlins Racing public product documentation [18]) 29
Figure 3.4 SC24 vehicle model in VI-CarRealTime simulation environment 30
Figure 3.5 dSPACE MicroAutoBox II used for onboard acquisition and control (source: dSPACE [15]) 32
Figure 3.6 SBG Systems Ellipse-N inertial navigation system (source: SBG Systems [16]) 32
Figure 3.7 Kistler CORREVIT S-Motion Standard (source: Kistler [19]) 33
Figure 3.8 RLS RM08 magnetic steering-angle encoder (source: RLS [17]) 34
Figure 3.9 Measured and simulated longitudinal and lateral acceleration during the steering-frequency sweep 36
Figure 3.10 Measured and simulated sideslip angle and steering-wheel angle during the steering-frequency sweep 37
Figure 3.11 Measured and simulated wheel speeds during the steering-frequency sweep 37
Figure 3.12 Measured and simulated yaw rate and lateral acceleration during the steering-frequency sweep 38
Figure 3.13 Measured and simulated longitudinal and lateral acceleration during the double lane change 38
Figure 3.14 Measured and simulated yaw rate and sideslip angle during the double lane change 39
Figure 3.15 Measured and simulated wheel speeds during the double lane change 39
Figure 3.16 Measured and simulated vehicle speed and steering-wheel angle during the double lane change 40
Figure 3.17 Measured and simulated longitudinal and lateral acceleration during the slalom 41
Figure 3.18 Measured and simulated yaw rate and lateral acceleration during the slalom 41
Figure 3.19 Measured and simulated sideslip angle during the slalom 42
Figure 3.20 Measured and simulated wheel speeds during the slalom 43
Figure 4.1 Damper-velocity and roll-rate distributions over the reference lap 46
Figure 4.2 Selected damper force-velocity characteristics implemented in the vehicle model 48
Figure 4.3 Nonlinear quarter-car step response for the selected damper characteristics 50
Figure 4.4 Linearised two-degree-of-freedom vertical frequency response of the selected configurations 51
Figure 4.5 Equivalent roll damping ratio estimated from the secant damping coefficient 52
Figure 4.6 Nonlinear roll step response for the selected damper characteristics 53
Figure 5.1 Empirical frequency-response estimate from steering-wheel angle to lateral acceleration 56
Figure 5.2 Empirical frequency-response estimate from steering-wheel angle to yaw rate 57

Figure 5.3 Empirical frequency-response estimate from steering-wheel angle to sideslip angle 57
Figure 5.4 Empirical frequency-response estimate from lateral acceleration to sideslip angle 58
Figure 5.5 Empirical frequency-response estimate from lateral acceleration to roll angle 58
Figure 5.6 Empirical frequency-response estimate from steering-wheel angle to roll angle 59
Figure 5.7 Empirical frequency-response estimate from lateral acceleration to yaw rate 60
Figure 5.8 Lap-time variation relative to Set 1 62
Figure 5.9 Vehicle-speed distribution over the simulated laps 63
Figure 5.10 Spatial histories of steering-wheel angle, sideslip angle and vehicle path over the reference lap 64
Figure 5.11 Bin-averaged steering-wheel angle and sideslip angle versus lateral acceleration 65
Figure 5.12 Virtual-driver command activity and sideslip-angle indicators 66
Figure 5.13 Steering-wheel torque and mechanical-work indicators 67
Figure 5.14 Number of wheel-lift onsets for each damper set 68
Figure 5.15 Longitudinal and lateral acceleration at wheel-lift onset 69

List of Tables

Table 1.1 Main vehicle parameters of the SC24 prototype 13
Table 4.1 Low-speed equivalent damping ratios for the six selected sets 48
Table 5.1 Wheel-lift count and duration metrics for the six damper sets 68

1 Introduction

Developing a Formula Student car requires a continuous compromise between performance targets, budget and the limited time available before the international competitions.
Within these constraints, this work focuses on making better use of the hardware already installed on SC24. The specific objective is to define a sound baseline tuning for the passive hydraulic dampers used with the car's double-wishbone suspension, reducing the amount of trial-and-error track testing.

1.1 Formula Student



Figure 1.1 Formula Student teams at an international event

Formula Student is an international engineering design competition in which university teams conceive, design, manufacture, test and compete with a single-seater formula-style race car [1].
Although the dynamic performance of the vehicle is an important part of the final result, the competition is not intended to reward only the fastest car. Instead, the objective is to evaluate the complete engineering project and design flow: the design process, the technical quality of the vehicle, the cost and manufacturing strategy, the business case, the reliability of the prototype and the ability of the team to operate under strict deadlines and resource constraints.

The format of the competition reproduces, in a simplified but highly demanding way, the development cycle of a motorsport prototype. Each team is required to define performance targets, design the vehicle architecture, manufacture and assemble the car, validate the main systems through testing, document the design decisions and finally

demonstrate the vehicle's actual capabilities on track. For this reason, Formula Student is widely regarded as one of the most complete educational experiences available to engineering students, since it combines vehicle dynamics, structural design, powertrain development, electronics, controls, aerodynamics, manufacturing, project management, budgeting and technical communication within a single project.

The competition originated from the Formula SAE concept developed in the United States in the 1980s and later expanded to Europe. The present European calendar includes several national and international events, each conducted under a common technical and sporting framework [1].

A key feature of Formula Student is that the car must be mainly conceived and developed by students. External support from sponsors, suppliers, university laboratories and industrial partners is common and often necessary, but the engineering responsibility remains within the student team. This aspect gives the competition a strong educational value: students are not only required to produce a functioning vehicle, but also to justify their design choices in front of experienced judges from the automotive and motorsport industries. Therefore, an efficient team structure, good documentation, design reviews, testing procedures and knowledge transfer between generations of students are essential to maintain competitiveness over multiple seasons.

Formula Student includes internal-combustion, electric and driverless categories, depending on the event. SC24 competes as an electric vehicle; its development therefore combines the mechanical design of the prototype with a high-voltage powertrain, embedded control and data acquisition [1].

Before being allowed to compete in the dynamic events, each vehicle must pass a series of technical inspections. These inspections are fundamental because the cars are prototypes built by students, often with highly customised solutions. The inspection process checks the compliance of the vehicle with the rules and especially verifies the safety of the main systems, including the chassis, driver equipment, braking system, electrical system, accumulator, shutdown circuit and, for autonomous vehicles, the additional safety systems required for driverless operation.
This procedure also reflects one of the main principles of the competition: performance is only relevant if achieved within a safe, reliable and rule-compliant engineering framework.

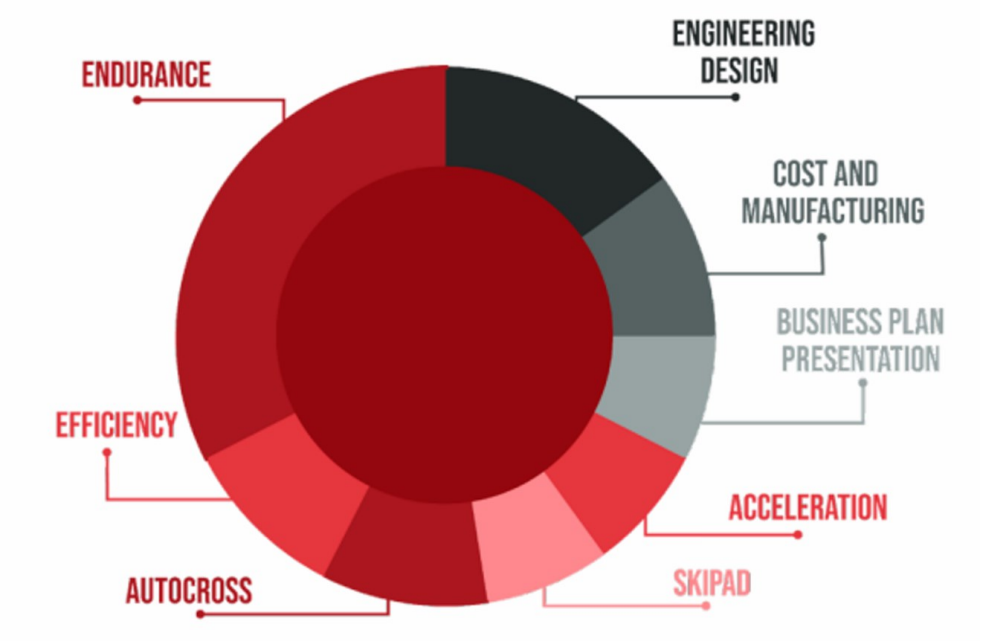


Figure 1.2 Static and dynamic event categories in Formula Student (adapted from [1])

The total score is divided into static and dynamic events. The static events evaluate the entire engineering design flow without considering the pure lap time, while the dynamic events assess the actual performance of the car on track. This scoring structure forces the teams to develop a balanced vehicle and a balanced organisation. A very fast car with poor reliability, insufficient documentation or weak design justification will not necessarily win the competition. Similarly, a technically elegant car that cannot complete the dynamic events will lose a large part of the available points. The winning team is therefore usually the one that achieves the best compromise between performance, robustness, manufacturability, cost awareness and engineering maturity.

1.2 Static Events

The static events are Engineering Design, Cost and Manufacturing, and Business Plan Presentation.
In the Engineering Design event, the team presents the complete technical development of the vehicle. The judges analyse the main design choices, the validation methods, the use of simulations and testing, the integration between subsystems and the consistency between the initial targets and the final prototype. This event is particularly important because it rewards not only innovative solutions, but also the ability to prove that a design decision is justified by calculations, simulations, experimental data or a clear engineering mindset.

The Cost and Manufacturing event evaluates the economic and production aspects of racing. Teams are required to prepare a detailed cost report and to justify the manufacturing processes, materials and components used in the vehicle. The objective is not simply to minimise the cost, but to demonstrate awareness of production

constraints, process selection, bill of materials, manufacturability and, in recent editions, also sustainability-related aspects such as carbon footprint and environmental impact. This event is useful because it forces the students to consider that engineering performance must be achieved within economic and industrial constraints.

The Business Plan Presentation simulates the presentation of a business case to potential investors or industrial partners. The team must propose a product, service or business model derived from the vehicle or from one of its technologies and must support the idea with a credible analysis of the market, customers, competitors, costs, revenues and implementation strategy. Although this event is less directly connected to vehicle dynamics, it is an important part of the competition because it develops communication, entrepreneurship and financial planning skills. It also reinforces the idea that a racing prototype is not only a technical object, but the result of an integrated product-development process.

1.3 Dynamic Events

The dynamic events traditionally include Acceleration, Skidpad, Autocross, Endurance and Efficiency. Each of them highlights a different aspect of vehicle performance. The Acceleration event consists of a straight-line sprint over a distance of 75 m. It mainly evaluates traction capability, power delivery, mass distribution, launch control, tyre utilisation and the calibration of the drivetrain control system. In electric four-wheel-drive vehicles, the result is strongly influenced by the ability to distribute torque between the wheels without exceeding the available tyre-road friction.

The Skidpad event is designed to evaluate lateral grip in quasi-steady-state cornering. The track is shaped as a figure of eight, composed of two pairs of concentric circles. The vehicle performs laps in both directions, and the timed laps are used to calculate the final result. This event is particularly sensitive to tyre performance, mass, centre of gravity height, lateral load transfer distribution, suspension kinematics, roll stiffness distribution, roll-centre height, aerodynamic downforce at low speed and the ability of the driver or controller to maintain the car close to the limit. Since the manoeuvre is highly repeatable, it is often used during the design phase as a reference case for vehicle dynamics simulations and setup optimisation.

The Autocross event consists of a single lap on a cone-defined handling track. The layout typically includes short straights, slaloms, chicanes, hairpins and corners with different radii. Compared with Skidpad, Autocross is more transient and requires the vehicle to perform well during combined braking, corner entry, rotation, traction at corner exit and rapid direction changes. It is also the first dynamic event that gives a complete indication of the vehicle's lap-time potential. For this reason, it is strongly influenced by the overall balance of the car, the confidence provided to the driver, the damping setup, the steering response, the tyre warm-up behaviour and the robustness of the control systems.

Endurance is usually the most important dynamic event because it combines performance, reliability and energy management. The event covers approximately 22 km and is driven by two drivers, with a driver change after roughly half distance. Completing Endurance requires the vehicle to operate continuously for a much longer time than in the other dynamic events. Components that may appear acceptable during

short tests can become critical due to thermal loads, mechanical fatigue and electrical issues. For electric vehicles, the event also requires careful management of the available energy, regenerative braking, and the thermal behaviour of the accumulator, inverters and motors. Therefore, Endurance is often the event that best reveals the overall maturity of the vehicle and of the team's testing process.

The Efficiency score is connected to Endurance and evaluates how effectively the car uses fuel or electrical energy in relation to its performance. This prevents the competition from rewarding only maximum power or aggressive energy consumption. A competitive vehicle must be fast, but it must also use the available energy intelligently. In this sense, the Efficiency event encourages teams to optimise not only the mechanical design, but also the control strategy, aerodynamic drag, drivetrain losses, regenerative braking and driving style.

1.4 Competitive and Technical Context

In recent years, the technical level of Formula Student vehicles has increased significantly. The best electric cars are lightweight prototypes, often equipped with carbon-fibre monocoques, 10-inch slick tyres, active aerodynamic packages, telemetry systems, torque vectoring, traction control and highly optimised suspension layouts. The most advanced teams design many components in-house, including wheel hubs, uprights, planetary gearboxes, inverters, battery containers, aerodynamic devices and sometimes even electric motors. Additive manufacturing, composite structures, topology optimisation, lap-time simulation, multibody simulation, CFD and hardware-in-the-loop testing are widely used tools in the development process.

This high level of technical freedom makes Formula Student a particularly interesting environment for vehicle dynamics research. The regulations impose strict safety and dimensional constraints but still allow a wide range of design solutions. Consequently, teams can investigate concepts that would be difficult to test in conventional production vehicles, such as hydraulically interconnected suspensions, mode-decoupled suspension systems, aggressive aerodynamic platforms, torque-vectoring strategies and advanced driver-in-the-loop simulation workflows. The competition therefore acts as a practical laboratory where innovative solutions can be designed, manufactured, tested and compared under real operating conditions.

Suspension design and damper tuning are especially important in Formula Student because the cars operate on tight and highly transient tracks, where the average speed is relatively low compared with professional circuit racing, but the frequency of steering, braking and acceleration inputs is very high. The suspension system must provide mechanical grip, control the tyre load variations, maintain a stable aerodynamic platform when an aero package is present and give the driver a predictable response. In this context, the damper setup has a direct influence on transient balance, wheel load control, response to bumps and surface irregularities, pitch and roll motion, traction and driver confidence. For this reason, the analysis and optimisation of damping characteristics is a relevant topic in the development of a Formula Student prototype.

At European level, several teams have become reference points because of their technical solutions and consistent results. Examples include AMZ Racing from ETH Zurich, FS Team Tallinn from Tallinn University of Technology and Tallinn University of Applied Sciences, TUfast from the Technical University of Munich, Rennteam Uni Stuttgart, Joanneum Racing Graz, TU Graz Racing and other teams that frequently compete at the top of the main European events. Their vehicles often represent the state of the art of the competition, with highly integrated electric powertrains, advanced control systems, carbon structures, efficient aerodynamic packages and extensive use of simulation and testing.

1.5 SC24 Overview



Figure 1.3 SC24 Formula Student prototype

Table 1.1 Main vehicle parameters of the SC24 prototype

Vehicle main data	
Mass without driver	211 kg
Front mass repartition	47.5 %
Wheelbase length	1.525 m
Front and rear tracks width	1.202 m
Centre of Gravity height from ground	0.28 m
Tyres	185/40 R13 slick
Rims	R13 magnesium-aluminium alloy
Aerodynamic Lift coefficient	4.78
Aerodynamic Drag coefficient	1.48
Nominal HV battery pack capacity	7.7 kWh
Nominal HV battery pack voltage	574.2 V

The vehicle chassis consists of a sandwich monocoque structure made of carbon-fiber-reinforced polymer (CFRP) skins with an aluminium honeycomb core. The primary structure is complemented by aluminium and steel anti-rollover members, while energy absorption in frontal impacts is ensured by an aluminium honeycomb impact attenuator.
The suspension system adopts a double wishbone architecture at both the front and rear axles, featuring a fully adjustable push-rod layout acting on longitudinally mounted spring-damper units. The pushrods are manufactured from CFRP tubes and are connected to the monocoque and to the machined aluminium uprights through spherical (uniball) joints, allowing precise kinematic control and setup flexibility.
The powertrain is fully electric and based on the AMK Formula Student racing kit. It comprises four independent electric drive units, each consisting of an IGBT-based inverter and a surface permanent magnet / interior permanent magnet (SPM–IPM) electric motor. Each motor is independently controlled and is capable of delivering a maximum torque of 21 Nm and a maximum rotational speed of 20,000 rpm, corresponding to a peak power of up to 35 kW per unit. The overall system can theoretically provide up to 140 kW at a DC voltage level of 600 V; however, in compliance with Formula Student Germany regulations, the maximum power drawn from the DC battery bus is limited to 80 kW.
The motors are mounted in an outboard in-wheel configuration and transmit torque to the wheels through a two-stage planetary gearbox with a fixed transmission ratio of 14.69:1.
The high-voltage energy storage system uses a lithium-polymer battery pack with a nominal capacity of 7.7 kWh and a nominal voltage of 574.2 V.

1.6 Thesis Outline

Chapter 2 provides the theoretical background required to analyse and tune the suspension system of a Formula Student prototype, with specific focus on the vehicle dynamics aspects directly related to damper characteristics. The chapter reviews the main mechanisms governing grip, load transfer, roll and pitch dynamics, and introduces the physical interpretation of hydraulic damper force-velocity characteristics.
Chapter 3 describes the VI-CarRealTime model and its validation. Steering, braking and wheel-torque signals measured on track are replayed through MATLAB/Simulink co-simulation. The simulated longitudinal and lateral acceleration, yaw rate, sideslip angle, wheel speeds and vehicle speed are compared with telemetry to assess whether the model reproduces the main behaviour of SC24.
Chapter 4 presents the experimental characterisation of the passive hydraulic dampers. Dynamometer force-velocity curves are analysed in compression and rebound. An equivalent low-speed damping ratio at a reference shaft velocity of 20 mm/s is used only as a preliminary screening indicator, because this operating region is relevant to the control of the main body motions. Six representative characteristics are retained for the vehicle-level comparison.
Chapter 5 presents the vehicle level comparison between the selected damper sets. The comparison focuses on handling balance, wheel load behaviour, and performance-related metrics, including cornering capability and lap time sensitivity. The analysis includes a standardised steering chirp and complete hot laps performed by a virtual driver. The configurations are compared in terms of frequency response, lap time, vehicle sideslip, driver-control activity, steering-wheel mechanical work and wheel-lift occurrence and duration.

Chapter 6 summarises the main outcomes, discusses the limitations of the adopted method and prospects for future development.

1.7 Objectives

The main objective of this thesis is to improve the dynamic performance of the SC24 Formula Student electric prototype by optimising the setup of its passive hydraulic dampers, without changing the suspension hardware or introducing active systems, since they are forbidden by the rules.
The work aims to exploit the available suspension components under the operating conditions of Formula Student Autocross and Endurance events, which are characterised by frequent transients, combined lateral and longitudinal loading and repeated small road disturbances.
More specifically, the objectives of the thesis can be summarised as follows:

- To identify a damper setup that improves mechanical grip by managing transient vertical tyre loads without compromising vehicle balance.
- To reduce the occurrence and duration of wheel-lift events while recognising that total quasi-steady load transfer is governed by vehicle equilibrium and cannot be eliminated through damping alone.
- To control the development of load-transfer transients without introducing abrupt chassis reactions, oscillations or loss of control.
- To establish a structured and physically motivated methodology for damper setup selection, based on the analysis of force–velocity characteristics and their influence on vehicle-level behaviour. Rather than relying on trial-and-error approaches, the objective is to reduce the number of configurations to be tested by identifying those that are theoretically well-suited to the target application.
- To validate the effectiveness of the proposed damper setup through simulation, using a virtual vehicle model previously validated against on-track telemetry data. The comparison is carried out in terms of handling balance, wheel load behaviour, wheel lift occurrence, and performance-related indicators such as cornering capability and lap time sensitivity.

Overall, the objective of this work is not only to identify a specific damper configuration for the studied prototype, but also to demonstrate how a validated virtual model, combined with a sound understanding of suspension dynamics, can be used as a reliable tool to guide damper tuning decisions in a motorsport context.

2 Theoretical Foundations

Vehicle dynamics covers every interaction among the driver, the vehicle and the road. This chapter deliberately considers only the part of that subject needed to interpret the present work: how tyre forces depend on vertical load, how a suspension distributes and transmits that load, how the sprung and unsprung masses respond in time and frequency, and how a nonlinear damper modifies that response. The sequence is important. A damper does not generate steady-state grip by itself; it changes the motion of the vehicle and the time history of the loads through which the tyres generate force. The simple analytical models introduced below are therefore used as interpretative tools. The complete Formula Student prototype remains a nonlinear, coupled multibody system and is evaluated with the vehicle model described in the following chapters [2,5,8-10].

2.1 Tyre Forces and Load Transfer

2.1.1 Tyre force generation and load sensitivity

The tyre is the only component that exchanges longitudinal and lateral forces with the road. Its force capability depends on vertical load, longitudinal slip, slip angle, camber, pressure, temperature and surface conditions. Under pure lateral slip, the initial slope of the lateral-force curve defines the cornering stiffness, while the maximum of the curve defines the peak lateral force. Combined braking or driving and cornering further couples the available longitudinal and lateral forces. A complete tyre model accounts for all these variables; for the present discussion, the relevant point is the dependence on vertical load [2].

Experimental tyre behaviour is *load-sensitive*: increasing vertical load increases the absolute peak force, but less than proportionally. Equivalently, the global friction coefficient decreases as load increases. If the peak lateral force of one tyre is denoted by $f(F_z)$, this behaviour can be written schematically as

$$F_{y,\max} = f(F_z) = \mu_y(F_z)F_z, \qquad \frac{\mathrm{d}\mu_y}{\mathrm{d}F_z} < 0, \qquad f(F_{z0} - \Delta F_z) + f(F_{z0} + \Delta F_z) < 2f(F_{z0}). \tag{2.1}$$

The last inequality compares two tyres carrying the same total load. With equal loading, each tyre carries F_{z0}. After a lateral load transfer, one carries $F_{z0} + \Delta F_z$ and the other $F_{z0} - \Delta F_z$. Because $f(F_z)$ is concave over the relevant range, the gain of the more heavily loaded tyre is smaller than the loss of the unloaded tyre. Load transfer therefore reduces the maximum combined force that the axle can produce, even though the total vertical load on that axle is unchanged [2].

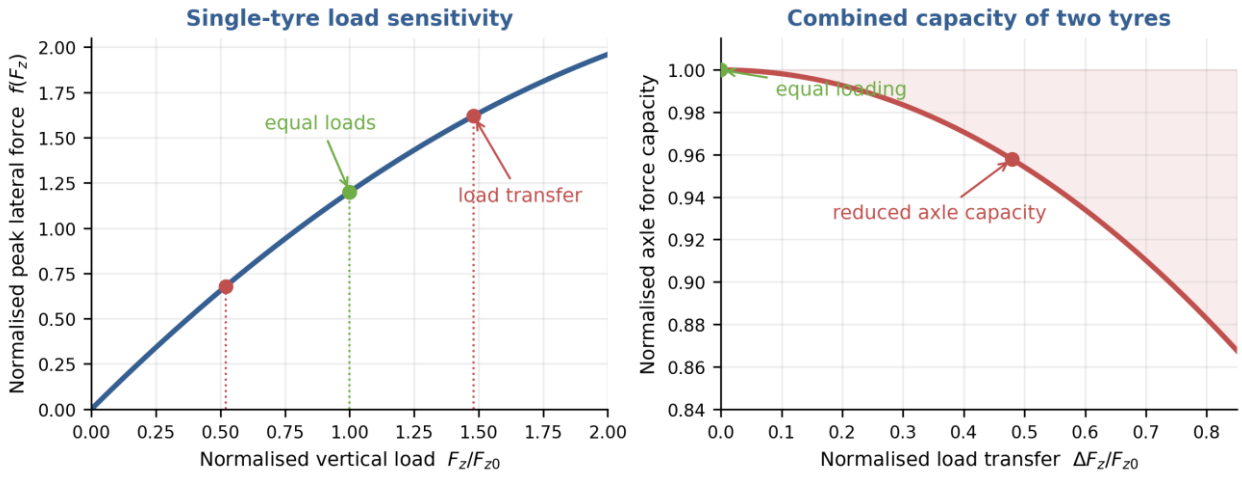


Figure 2.1 Schematic effect of tyre load sensitivity on the combined force capability of an axle. The curves are illustrative rather than tyre-specific; author's elaboration based on [2].

This result explains why vertical-load distribution and contact-load fluctuations are central to suspension tuning. It does not imply that the vehicle should be made arbitrarily soft: camber control, aerodynamic-platform control, suspension travel and transient response impose competing requirements. It does establish the physical link used throughout this thesis: a damper setting is beneficial only if the vehicle-level response allows the tyres to use their force capability more effectively and consistently.

2.1.2 Lateral load transfer and its distribution

During cornering, vertical load is redistributed from the inside tyres to the outside tyres. It is preferable to call this phenomenon *load transfer*, because vehicle mass is not transferred. Let $\Delta F_{z,i}$ denote, at axle i, the increase of the outside-wheel load and the equal decrease of the inside-wheel load. Neglecting small higher-order terms, moment equilibrium for a two-axle vehicle gives

$$t_F \Delta F_{z,F} + t_R \Delta F_{z,R} = m a_y h + I_{xz} \dot{r} \simeq m a_y h, \tag{2.2}$$

where t_F and t_R are the tracks, m is vehicle mass, h is the height of its centre of gravity, a_y is lateral acceleration and r is yaw rate. Equation (2.2) fixes the overall amount of quasi-steady lateral load transfer. Consequently, lowering the centre of gravity or increasing track width reduces the transfer required for a given lateral acceleration. Changing springs, anti-roll bars or dampers does not remove the equilibrium requirement; these elements mainly change how the total is divided between the two axles and how that division develops during a transient [2-4].

The physical paths that produce the load change must nevertheless be distinguished. In a first-order axle model, the contribution associated with the sprung mass can be separated into a geometric part, transmitted through the suspension links, and an elastic part, transmitted through springs and anti-roll bars. During a transient, the dampers add a rate-dependent contribution. The unsprung masses supply a further component. A compact, deliberately simplified representation is

$$t_i \Delta F_{z,i} \simeq F_{y,s,i} q_i + K_{\phi s,i} \phi_i + C_{\phi,i} \dot{\phi}_i + m_{u,i} a_y h_{u,i}, \tag{2.3}$$

where q_i is the first-order no-roll-centre height, $K_{\phi s,i}$ is the suspension roll stiffness, $C_{\phi,i}$ is the corresponding installed roll-damping coefficient, and $h_{u,i}$ is the unsprung-mass centre-of-gravity height. The exact expressions include tyre compliance, the front-to-rear

distribution of lateral force, suspension kinematics, jacking forces and compliance effects; Equation (2.3) is intended only to expose the distinct load paths [2-4].

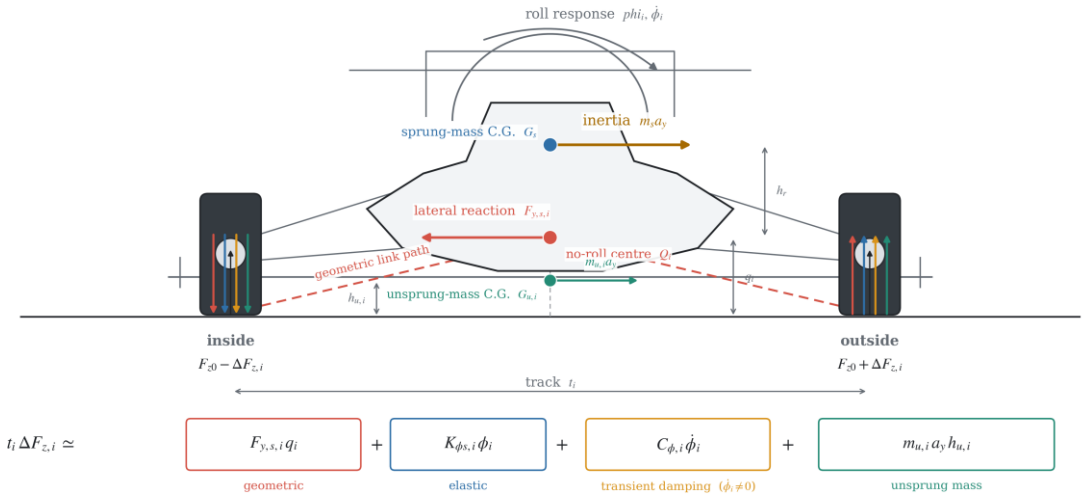


Figure 2.2 First-order decomposition of lateral load transfer at one axle into the sprung-mass geometric, elastic and transient damping contributions and the unsprung-mass contribution; author's elaboration based on [2-4].

Body roll is therefore not the cause of the total load transfer. Both roll and load transfer are responses to the same lateral-force and moment balance. Roll stiffness determines how much the body rotates and strongly influences the front-to-rear elastic distribution, while the geometric component depends on the suspension kinematics. Tyre vertical compliance acts in series with the suspension and also contributes to the measured body roll. These distinctions are especially important when comparing damper settings: a damper may noticeably alter the load history during corner entry and exit even though its force tends to zero in a truly steady turn [2-4].

2.1.3 Lateral response, roll and pitch transients

The main lateral-response variables used later in this thesis are lateral acceleration a_y, yaw rate r, sideslip angle β and sprung-mass roll angle ϕ. If u and v are the longitudinal and lateral velocities at the reference point, their first-order kinematic relationship is

$$\beta \simeq \frac{v}{u}, \qquad a_y = \dot{v} + ur \simeq u(\dot{\beta} + r). \tag{2.4}$$

These variables describe different parts of the same manoeuvre. Yaw rate quantifies the rotational response, sideslip quantifies the direction of travel relative to the vehicle heading, and lateral acceleration reflects the net lateral force. Their amplitudes and phase delays during a steering sweep are consequently useful measures of how faithfully the vehicle follows the driver's input [2].

The body motions that activate the suspension can be understood through modal coordinates. In heave the four corners move predominantly in the same direction; in roll the left and right sides move oppositely; in pitch the front and rear axles move oppositely; and in warp approximately opposite diagonal corners move together. For an isolated linear roll coordinate, the governing equation has the familiar second-order form

$$I_{\phi,s}\ddot{\phi} + C_{\phi}\dot{\phi} + K_{\phi,\mathrm{eff}}\phi = M_{\phi}(t) \simeq m_s a_y(t) h_r, \tag{2.5}$$

where $I_{\phi,s}$ is the sprung-mass roll inertia, h_r is the distance between the sprung-mass centre of gravity and the effective roll axis, and $K_{\phi,\mathrm{eff}}$ includes the relevant suspension and tyre stiffness. Pitch has an analogous form about the transverse axis. Equation (2.5)

makes the different roles of stiffness and damping explicit: stiffness reacts displacement and sets the quasi-steady angle, whereas damping reacts velocity and mainly controls overshoot, settling and phase during the transition [2,5].
At the instant of maximum roll angle, roll velocity may already be close to zero, so the roll-damper force can be small even while spring and anti-roll-bar forces are at their largest. Conversely, early in corner entry the roll angle is still small but roll velocity can be high, making the dampers a major part of the instantaneous load path. The same reasoning applies to pitch during braking and acceleration. Hence low-speed damping can change transient balance and driver perception without changing the final equilibrium demanded by Equation (2.2). Its effect on yaw rate and sideslip is indirect: the damper changes the time-dependent vertical loads, camber states and tyre forces, which then change the vehicle's lateral response [2-4,7].

2.2 From Suspension Geometry to Wheel-Domain Properties

2.2.1 Double-wishbone push-rod architecture

The suspension connects each wheel carrier to the chassis while allowing a prescribed wheel path. The SC24 prototype uses a double-wishbone layout with push-rods and inboard spring-damper units at both axles. The upper and lower wishbones constrain the upright and provide design freedom over camber, toe, caster, track, roll-centre location and their variation through wheel travel. These desirable properties are not automatic consequences of the architecture: they depend on the hard-point geometry, component stiffness and joint compliance [2,5,13].
The push-rod transmits wheel motion to a rocker, which rotates and compresses or extends the inboard spring-damper unit. Moving the unit inboard can improve packaging and reduce the mass directly carried by the upright. More importantly for this work, the rocker geometry establishes the kinematic transformation between wheel travel and damper travel. This transformation determines the force and velocity seen at the damper and therefore must be included before different force-velocity curves are compared at vehicle level [5,10,13].

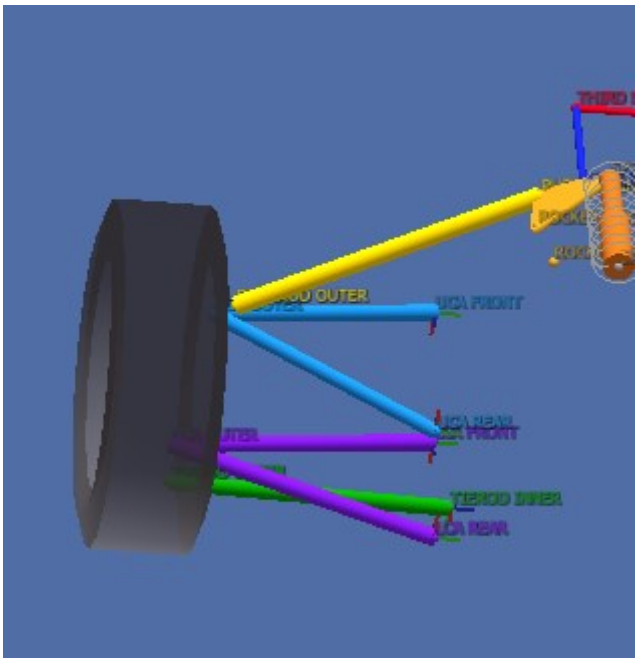


Figure 2.3 Double-wishbone push-rod suspension model generated in VI-SuspensionGen (author's screenshot; software by VI-grade [14])

2.2.2 Motion ratio, wheel rate and installed damping

Motion-ratio conventions vary in the literature. In this thesis it is defined explicitly as damper displacement divided by wheel-centre vertical displacement,

$$\mathrm{MR}(z_w) = \frac{\mathrm{d}z_d}{\mathrm{d}z_w}, \qquad v_d = \mathrm{MR}(z_w) v_w, \tag{2.6}$$

where z_d is the displacement along the damper axis and z_w is wheel vertical travel. The derivative notation emphasises that the ratio can vary through travel. Neglecting friction and compliance in the linkage, virtual work gives

$$F_w \, \mathrm{d}z_w = F_d \, \mathrm{d}z_d, \qquad F_w = \mathrm{MR} \, F_d. \tag{2.7}$$

For a linear spring of stiffness k_{sp} and a locally linear damper coefficient c_d, a constant motion ratio therefore produces the familiar wheel-domain quantities

$$k_w = k_{sp}\mathrm{MR}^2, \qquad c_w = c_d\mathrm{MR}^2. \tag{2.8}$$

The square appears because the motion ratio acts once on displacement or velocity and once again on force. If the motion ratio changes appreciably with travel, the local wheel rate also contains a geometric term,

$$k_w = \frac{\mathrm{d}F_w}{\mathrm{d}z_w} = k_{sp}\mathrm{MR}^2 + F_{sp}\frac{\mathrm{dMR}}{\mathrm{d}z_w}. \tag{2.9}$$

The second term depends on the spring force already present at the operating point and is the origin of part of the rising- or falling-rate behaviour of a rocker system. For a nonlinear damper, the installed force is more generally $F_w = \mathrm{MR} \, F_d(\mathrm{MR} \, v_w)$ at a fixed suspension position. Consequently, the force-velocity curves measured at the damper cannot be inserted directly into wheel-level damping-ratio calculations unless this kinematic transformation is applied. The same convention is used later when the six candidate damper curves are converted and compared [5,10,13].

2.2.3 Ride frequency, roll stiffness and coupled modes

A useful preliminary suspension metric is the undamped ride frequency associated with the predominantly vertical motion of the sprung mass. Tyre and suspension stiffness act approximately in series. For one corner, the effective ride rate k_r and the corresponding approximate frequency are

$$k_r = \frac{k_w k_t}{k_w + k_t}, \qquad f_r \simeq \frac{1}{2\pi}\sqrt{\frac{k_r}{m_s}}, \tag{2.10}$$

where k_t is tyre vertical stiffness and m_s is the sprung mass associated with the corner. If $k_t \gg k_w$, the ride rate approaches the wheel rate. Guiggiani notes that this approximation is less appropriate for formula cars, for which tyre and suspension stiffness may be of the same order; tyre compliance can then reduce the body-mode frequency substantially [2]. A higher ride frequency provides greater platform support and can permit lower ride height, but it also requires more force for a given displacement and can increase sensitivity to roughness. It is therefore a design outcome constrained by tyres, aerodynamics and travel, not a universal indicator of performance [2,5].

For an axle with equal left and right wheel rates and small roll angles, the suspension contribution to roll stiffness is approximately

$$K_{\phi s,i} \simeq \frac{k_{w,i} t_i^2}{2} + K_{\phi,\mathrm{ARB},i}, \qquad RG = \frac{\phi_{ss}}{a_y/g} \simeq \frac{m_s g h_r}{K_{\phi,\mathrm{eff}}}, \tag{2.11}$$

where RG is the roll gradient in radians per g, commonly converted to degrees per g. Tyre roll compliance reduces the effective stiffness seen by the body. The total stiffness controls the overall roll angle, while its front-to-rear distribution is a principal determinant of the elastic load-transfer distribution and therefore of the quasi-steady balance [2,5].

Ride-frequency and roll-gradient calculations are valuable for initial setup, but they should not be mistaken for independent physical modes of the complete car. With one conventional spring-damper unit at each wheel, every unit contributes simultaneously to heave, roll, pitch and warp. Front and rear vertical motions are also coupled through the sprung mass and pitch inertia. Thus a single click change modifies several modal damping ratios at once. This coupling explains why a setting that appears favourable in a one-degree-of-freedom calculation may produce an unwanted response in another mode, and why the final choice must be assessed with the complete vehicle [2,8,10].

2.3 Vertical Dynamics and Frequency-Domain Interpretation

2.3.1 Two-degree-of-freedom quarter-car model

The two-degree-of-freedom quarter-car model is the simplest representation that retains both sprung-mass and wheel-hop dynamics. It contains a sprung mass m_s, an unsprung mass m_u, a suspension spring k_s, a damper c_s, and a tyre represented by the vertical stiffness k_t. Tyre damping is normally much smaller than suspension damping and is neglected. All coordinates are perturbations about static equilibrium, so weight does not appear explicitly [2,5,10].

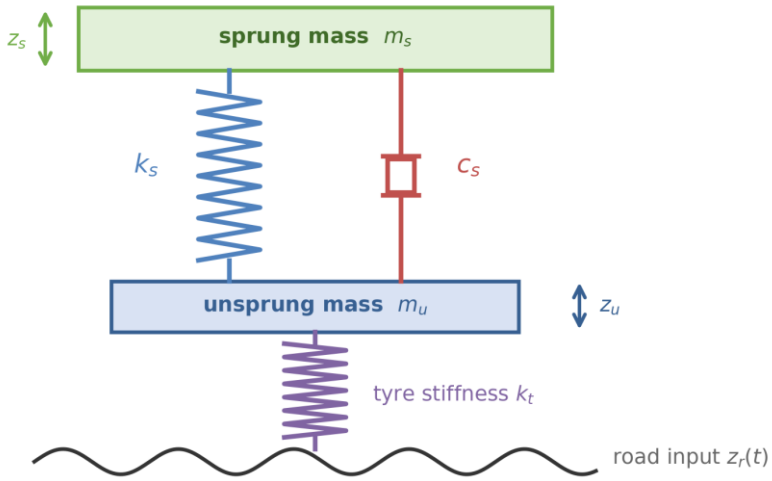


Figure 2.4 Linear two-degree-of-freedom quarter-car model used to interpret ride and road-holding behaviour; adapted from [2,5].

With the sign convention shown in Figure 2.4, the equations of motion are

$$\begin{aligned} m_s\ddot{z}_s + c_s(\dot{z}_s - \dot{z}_u) + k_s(z_s - z_u) &= 0, \\ m_u\ddot{z}_u + c_s(\dot{z}_u - \dot{z}_s) + k_s(z_u - z_s) + k_t(z_u - z_r) &= 0. \end{aligned} \tag{2.12}$$

Here $z_r(t)$ is the road displacement. A road wavelength λ encountered at constant longitudinal speed U excites the vehicle at $f = U/\lambda$; a general road can be decomposed into spatial harmonics and mapped to temporal frequencies in this way [2,10]. The model is linear only when k_s, c_s and k_t are constants. It therefore cannot reproduce the asymmetric and velocity-dependent damper curves studied in this thesis, but it remains useful for identifying the relevant modes, outputs and trade-offs before interpreting the nonlinear simulations.

2.3.2 Natural modes and damping ratio

Setting road input and damping to zero gives the undamped characteristic equation

$$m_s m_u \omega^4 - [m_s(k_s + k_t) + m_u k_s]\omega^2 + k_s k_t = 0. \tag{2.13}$$

Its two positive roots correspond to a lower-frequency body mode and a higher-frequency wheel-hop mode. Under the usual mass separation $m_s \gg m_u$, useful approximations are

$$\omega_b^2 \simeq \frac{k_s k_t}{(k_s + k_t)m_s}, \qquad \omega_h^2 \simeq \frac{k_s + k_t}{m_u}. \tag{2.14}$$

In the body mode the two masses move mainly in phase and the suspension and tyre compliances act approximately in series. In the wheel-hop mode the unsprung mass moves mainly against the tyre and suspension while the body moves much less. Reducing unsprung mass generally raises the wheel-hop frequency and reduces contact-load variation over a given disturbance, which is advantageous for road holding [2,5].

For a linear single-degree-of-freedom reference system, the critical damping coefficient and damping ratio are

$$c_{\text{crit}} = 2\sqrt{km}, \qquad \zeta = \frac{c}{c_{\text{crit}}}. \tag{2.15}$$

An underdamped free response has $0 < \zeta < 1$; $\zeta = 1$ is the fastest non-oscillatory response to an initial disturbance; and $\zeta > 1$ gives a slower overdamped response. These statements concern a particular linear mode and should not be converted into a universal damper target. A two-degree-of-freedom system has two modal damping ratios, obtained

from its complex eigenvalues, and a complete car has still more. The same physical dampers participate in all of them. In formula cars, where tyre stiffness is not overwhelmingly larger than suspension stiffness, increasing the damper coefficient can even couple the body more strongly to the tyre and degrade one response after another has improved, a condition commonly described as “locking” the damper [2,10].
The critical-damping concept is nevertheless useful for normalising candidate settings. Secant or tangent coefficients extracted from a nonlinear force-velocity curve can be transformed to the wheel and divided by a selected modal or corner critical coefficient. The resulting percentage describes a local operating point, not a constant property of the real damper and not the damping ratio of the complete vehicle.

2.3.3 Transmissibility, road holding and frequency response

The response to a harmonic input depends on excitation frequency as well as damping. For a base-excited single-degree-of-freedom system, the displacement transmissibility between mass motion X and road motion Y is

$$T_x(r,\zeta) = \left|\frac{X}{Y}\right| = \sqrt{\frac{1+(2\zeta r)^2}{(1-r^2)^2+(2\zeta r)^2}}, \qquad r = \frac{\omega}{\omega_n}. \tag{2.16}$$

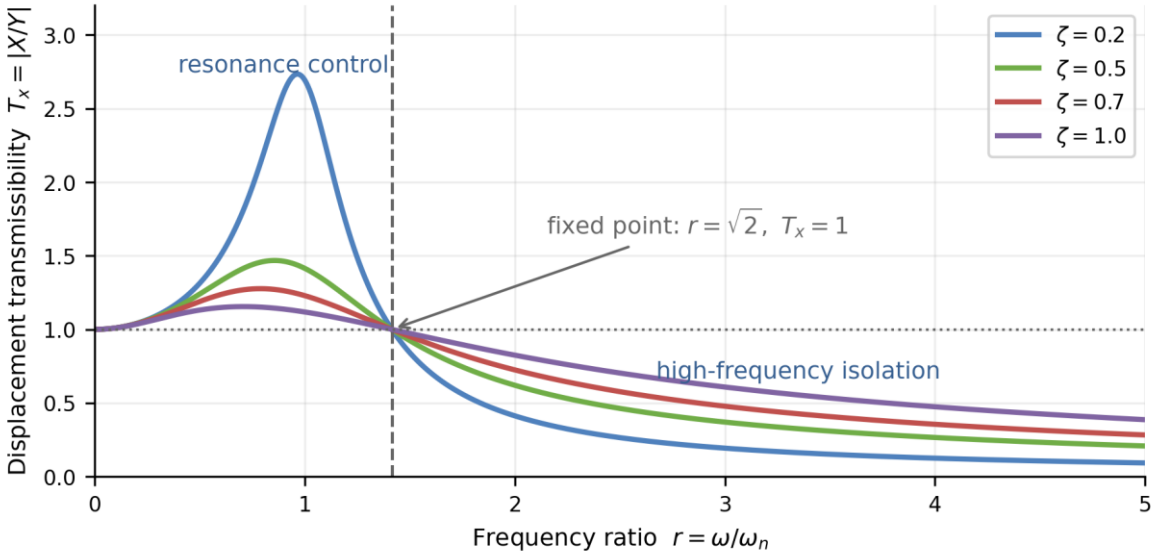


Figure 2.5 Displacement transmissibility of a base-excited single-degree-of-freedom system. All curves pass through $T_x = 1$ at $r = \sqrt{2}$; author’s calculation from Equation (2.16), based on [5].

Figure 2.5 exposes the basic compromise. Increasing damping suppresses the resonance peak and improves control around the body mode. Above the fixed point $r = \sqrt{2}$, however, it increases transmitted motion relative to a more lightly damped system and weakens high-frequency isolation. The crossing is a frequency ratio, not a fixed frequency in hertz. Moreover, damper shaft speed depends on both frequency and response amplitude; the low-speed/high-speed hydraulic transition cannot be inferred from excitation frequency alone [5,8,9].
For a race car, body acceleration is not the only relevant output. In the quarter-car model the fluctuating component of contact-patch load is, up to the chosen sign convention,

$$\Delta F_z = k_t(z_u - z_r). \tag{2.17}$$

Small body acceleration is associated with isolation of the sprung mass, whereas small ΔF_z indicates more uniform road contact. These objectives do not have the same optimum damping over the entire frequency range. Guiggiani consequently separates comfort,

based mainly on sprung-mass acceleration, from road holding, based on tyre-force fluctuations; the latter is the more relevant criterion for a racing application [2]. Formula SAE studies likewise show that strong low-frequency chassis control and low high-frequency tyre-load variation can require different effective damping levels [6,8,10].
For a linear multi-degree-of-freedom model subjected to a sinusoidal input, the steady response can be written directly in the frequency domain as

$$\hat{\mathbf{q}}(\omega) = [-\omega^2\mathbf{M} + \mathrm{j}\omega\mathbf{C} + \mathbf{K}]^{-1}\mathbf{B}\,\hat{x}(\omega), \qquad H_{yx}(\mathrm{j}\omega) = \frac{\hat{y}(\omega)}{\hat{x}(\omega)}. \quad (2.18)$$

The complex transfer function H_{yx} provides both gain and phase. This is why a swept-sine manoeuvre is informative: it excites a range of frequencies and allows the dynamic relationship between steering input and outputs such as yaw rate, lateral acceleration, sideslip and roll to be compared. For measured data, the H_1 spectral estimate and the magnitude-squared coherence are commonly written as

$$\widehat{H}_1(f) = \frac{G_{xy}(f)}{G_{xx}(f)}, \qquad \gamma_{xy}^2(f) = \frac{|G_{xy}(f)|^2}{G_{xx}(f)G_{yy}(f)}, \qquad 0 \le \gamma_{xy}^2 \le 1. \quad (2.19)$$

Here G_{xx} and G_{yy} are auto-spectral densities and G_{xy} is the cross-spectrum. High coherence indicates that, at that frequency, the output is consistently related to the chosen input under the assumptions of the estimate; it does not by itself prove that the vehicle model is correct. The comparison must still consider gain, phase, operating condition, nonlinearities and measurement quality [9,10].

2.4 Hydraulic Dampers and Nonlinear Force-Velocity Behaviour

2.4.1 Origin of the damping force and four-way adjustment

A hydraulic damper dissipates mechanical energy by forcing oil through restricted flow paths as the piston moves. In a simple orifice interpretation, piston velocity generates a volumetric flow Q, the restriction generates a pressure difference Δp, and that pressure acts over an effective piston area. The approximate relationships are

$$Q \simeq A_p v_d, \qquad \Delta p \simeq \frac{\rho}{2}\left(\frac{Q}{C_d A_o}\right)^2, \qquad F_d \simeq A_e \Delta p + F_f. \quad (2.20)$$

The expression is explanatory rather than a complete damper model. The effective flow area A_o changes when shim stacks deflect or auxiliary valves open; the compression and rebound chambers have different effective areas; seals add friction; and gas pressure, oil temperature, aeration and cavitation can alter the measured force. These mechanisms make a real force-velocity relationship nonlinear, asymmetric and history-dependent [6,12,18].
At small shaft velocities, much of the oil passes through bleed passages controlled by needle valves. As velocity and pressure rise, preloaded shim stacks or separate high-speed valves open and increase the effective flow area. This change produces the visible “knee” between low-speed and high-speed regions of the force-velocity curve. The terms *low speed* and *high speed* always refer here to damper shaft velocity, not vehicle speed. Slow chassis motions often populate the low-speed region, while kerbs and short-wavelength road inputs often create higher shaft velocities, but the association is not exact: a sufficiently large low-frequency motion can also generate high shaft speed [6,8,12].
The TTX25 units fitted to SC24 provide four external adjustments: low-speed compression, high-speed compression, low-speed rebound and high-speed rebound [18]. Compression and rebound are physically separate flow directions, while low- and high-speed adjustments mainly act on different flow regimes. Their effects are not perfectly

independent, because every adjustment changes the hydraulic network through which the same oil flows. The measured dynamometer curve, rather than the nominal click position alone, is therefore the appropriate description of each setting.

2.4.2 Quantifying nonlinear force-velocity curves

For a linear viscous element, $F_d = c_d v_d$ and one coefficient describes the complete curve. For a nonlinear damper, at least two local definitions are useful. At a specified non-zero velocity, the secant and tangent coefficients are

$$c_{\mathrm{sec}}(v_d) = \frac{F_d(v_d)}{v_d}, \qquad c_{\tan}(v_d) = \frac{\partial F_d}{\partial v_d}. \tag{2.21}$$

The secant coefficient gives the linear element that would produce the same force at that point. The tangent coefficient gives the incremental slope and is more closely related to the small perturbation around that operating condition. Both must be evaluated separately in compression and rebound and transformed through the motion ratio before they are compared with a wheel-domain critical coefficient. Near zero velocity, friction, offsets and sparse dynamometer breakpoints can make either measure unstable; a fitted local slope or a clearly stated reference velocity is therefore preferable to an unqualified single "damping coefficient" [6,8,12].

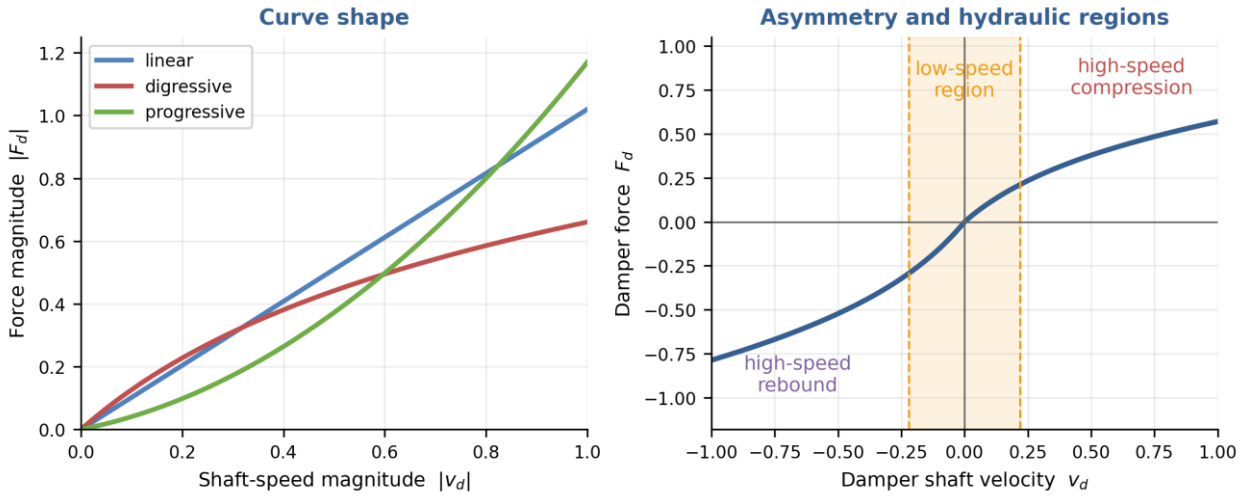


Figure 2.6 Idealised linear, digressive and progressive force-velocity laws, together with an asymmetric digressive characteristic and its hydraulic operating regions; author's elaboration based on [6,8,11,12].

An approximately linear curve has nearly constant slope. A digressive curve has a comparatively steep low-speed slope followed by a lower high-speed slope after the knee. This shape provides strong platform and transient control without allowing force to rise as rapidly over large shaft velocities. A progressive curve has increasing slope and can limit travel under severe compression events, although it can also produce large contact-load peaks if applied too aggressively. These labels describe the local shape over a stated velocity range; a real curve may be progressive in one region and digressive in another [6,8,11,12].

2.4.3 Compression-rebound asymmetry and vehicle-level implications

Compression damping resists shortening of the damper, whereas rebound damping resists extension. Racing dampers commonly use different forces in the two directions, often with more rebound than compression over part of the velocity range. This is a tuning choice rather than a universal optimum. Higher rebound force can control the release of

spring energy and restrain body motion, but excessive rebound can prevent an unloaded wheel from returning quickly enough after a bump or repeated disturbance. The suspension can then “pack down”, lose available travel and reduce contact-load consistency. Excessive high-speed compression can instead transmit a sharp force into both tyre and chassis, increasing load peaks and disturbing the vehicle over kerbs [6-8,12].

For a dissipative sign convention, the instantaneous damper power is non-negative and the energy converted into heat over one cycle is

$$P_d(t) = F_d(t)v_d(t) \geq 0, \qquad E_d = \int_0^T F_d\,(t)v_d(t)\,\mathrm{d}t = \oint F_d\,\mathrm{d}z_d. \tag{2.22}$$

Accordingly, dissipated energy is represented by the area of the force-displacement loop. A force-velocity hysteresis loop instead reveals dynamic lag and history dependence; its enclosed area is not itself the mechanical energy dissipated per cycle. Two dampers can therefore have similar mean force-velocity curves yet differ in hysteresis, temperature sensitivity or cycle-to-cycle behaviour [6,12].

The influence of each branch also depends on manoeuvre phase and axle. Low-speed compression and rebound affect the timing of roll and pitch load paths and can therefore modify entry response, yaw build-up and driver confidence. High-speed forces govern the compromise among wheel travel, body isolation and vertical tyre-load variation over roughness. In neither case is it generally valid to state that adding a given branch of damping always creates understeer or oversteer: the sign and magnitude depend on which wheels are moving in compression or rebound, the front-to-rear elastic distribution, tyre characteristics and the frequency content of the event [6-10].

This theoretical framework determines the methodology adopted later in the thesis. The available dynamometer curves are first described through their compression and rebound forces, knees and local secant and tangent coefficients. Those quantities are converted to the wheel domain through the measured motion ratio and compared with reference critical-damping levels. A limited set of representative nonlinear curves is then evaluated in the complete VI-CarRealTime model, using both controlled manoeuvres and road-related excitation. The final judgement is based on vehicle-level outputs—transient lateral response, body motion, suspension travel and contact-patch load variation—because no single coefficient or isolated mode can capture the full effect of a four-way damper on the SC24 prototype.

3 Formula Student Prototype and Virtual Vehicle Model

3.1 Vehicle Overview and Suspension Architecture

The vehicle considered in this study is an all-wheel-drive Formula Student electric prototype with four independently driven in-wheel motors. Its chassis is a carbon-fibre-reinforced polymer and aluminium-honeycomb sandwich monocoque, complemented by aluminium and steel rollover structures and an aluminium-honeycomb impact attenuator. The main suspension layout is shown in Figure 3.1.

The suspension system adopts a double wishbone layout at both the front and rear axles, actuated through a pushrod architecture. The pushrods are manufactured from CFRP tubes and connect the wheel uprights to inboard-mounted coilover units via spherical joints. This solution allows a reduction of unsprung mass and enables a compact packaging of the spring-damper assemblies within the chassis, while preserving a high degree of setup flexibility.

Both axles are equipped with coilover units consisting of linear springs and passive hydraulic dampers, mounted coaxially with the springs. Anti-roll stiffness is provided by T-bar anti-roll bars at both the front and rear axles, contributing to the control of roll motion and to the distribution of lateral load transfer between the two axles.

The suspension architecture is designed to operate with a motion ratio close to unity, ensuring that damper shaft velocities remain representative of wheel vertical motion. This limits leverage effects and reduces the number of physical components that may introduce mechanical compliance.

The front and rear layouts use the same basic architecture and hardware, while the vehicle has a rear-biased static mass distribution. In normal track operation this difference is addressed through axle-specific setup choices. In the present study it is retained in the vehicle model, but the same damper curve is deliberately applied at all four corners to limit the number of variables.

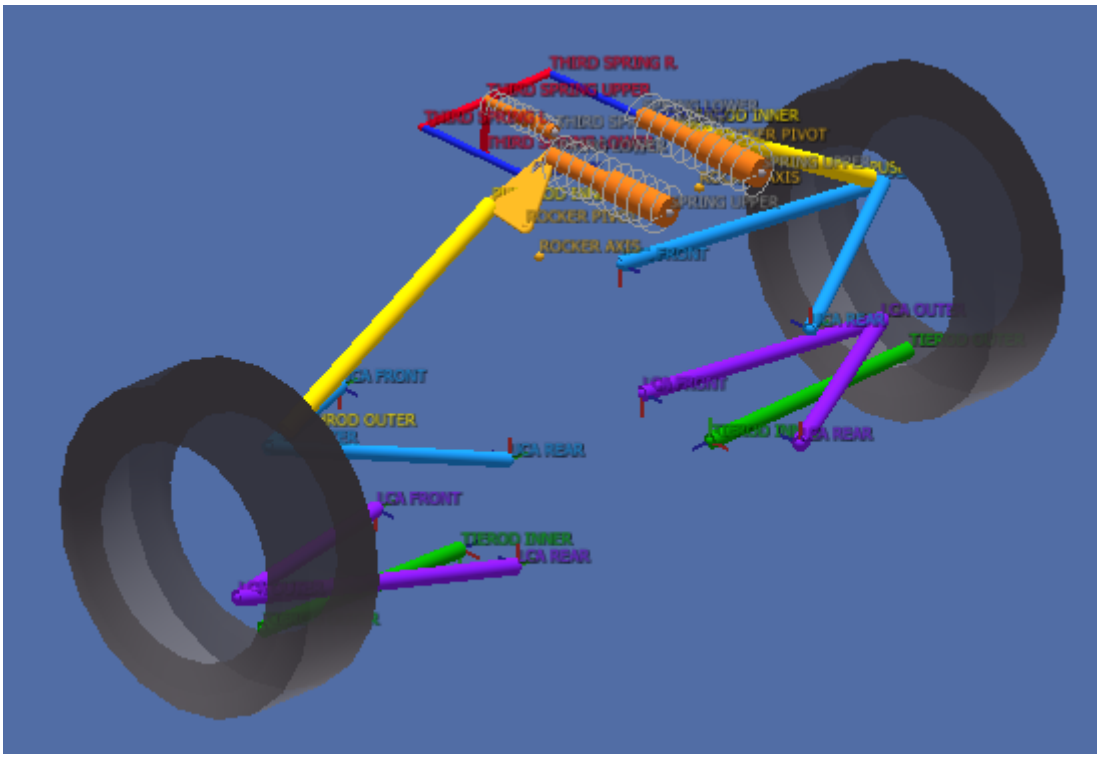


Figure 3.1 SC24 front suspension model and hard-point layout

3.2 Suspension Parameters and Damper Integration in the Virtual Model

The suspension parameters implemented in the virtual vehicle model are consistent with the physical characteristics of the real prototype.
At the time of the validation tests, the car was equipped with Öhlins TTX 25 MkII FSAE dampers, with separate low-speed and high-speed adjustments in compression and rebound. The damper and its adjustment circuits are shown in Figures 3.2 and 3.3 [18].
Linear springs with a nominal stiffness of 70 N/mm are used at all four corners.
The pushrod installation geometry results in a wheel-to-damper motion ratio close to unity also at the front axle, while slightly lower values are observed at the rear axle to compensate for the higher static load level. The motion ratio is treated in the model as a geometric property of the suspension layout and is implicitly accounted for in the VI-CarRealTime implementation.
Passive hydraulic dampers are represented through force-velocity lookup tables derived directly from the available dynamometer data.

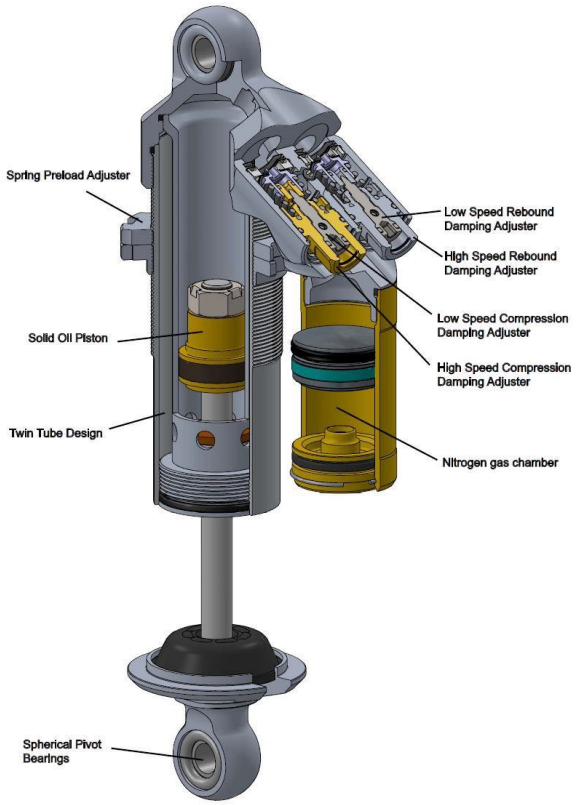


Figure 3.2 Öhlins TTX 25 MkII FSAE damper cutaway (source: Öhlins Racing public product documentation [18])

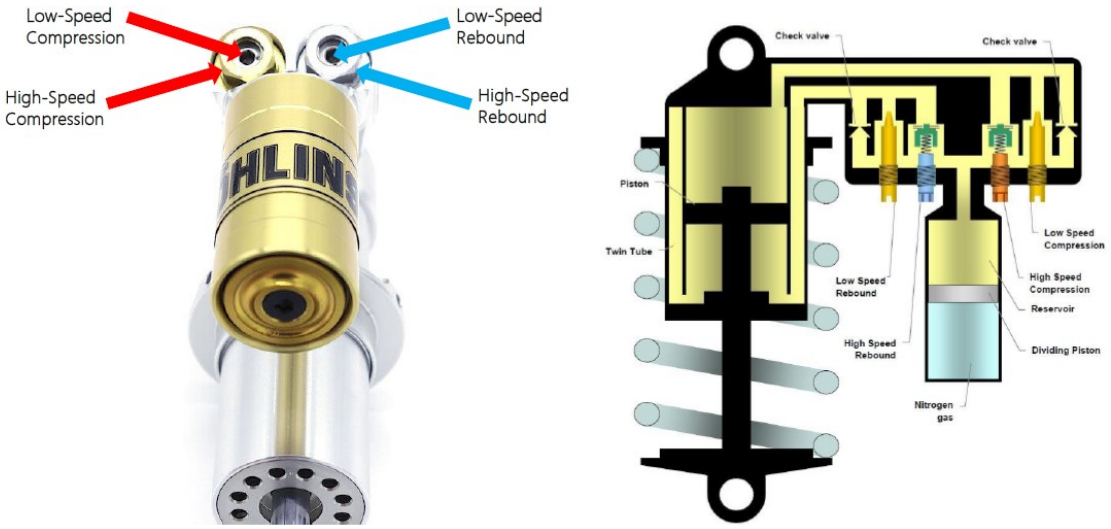


Figure 3.3 Compression and rebound adjustment circuits of the Öhlins TTX 25 MkII FSAE damper (source: Öhlins Racing public product documentation [18])

The damper characteristics are defined independently for compression and rebound and include separate regions for low-speed and high-speed operation. This formulation enables the nonlinear behaviour of the dampers to be accurately reproduced within the simulation environment and allows a direct implementation of the different damper setups analysed in this work.

A simplified setup strategy was adopted for this part of the work and for the subsequent: the same force-velocity characteristic was assigned to both axles and to all four corners. This has been implemented during track tests by closing all the set-up screws in order to insert the known characteristic in the virtual vehicle to validate, since there were no other meaningful data available for the set of damper actually used during track tests. Later on another identical set of damper has been freshly serviced by Lorandi Sospensioni, an historical supplier of the team, which also characterized the new set, supplying the baseline data for the next part of this work, in which the best set-up screws combination has been evaluated.

3.3 Virtual Vehicle Model in VI-CarRealTime

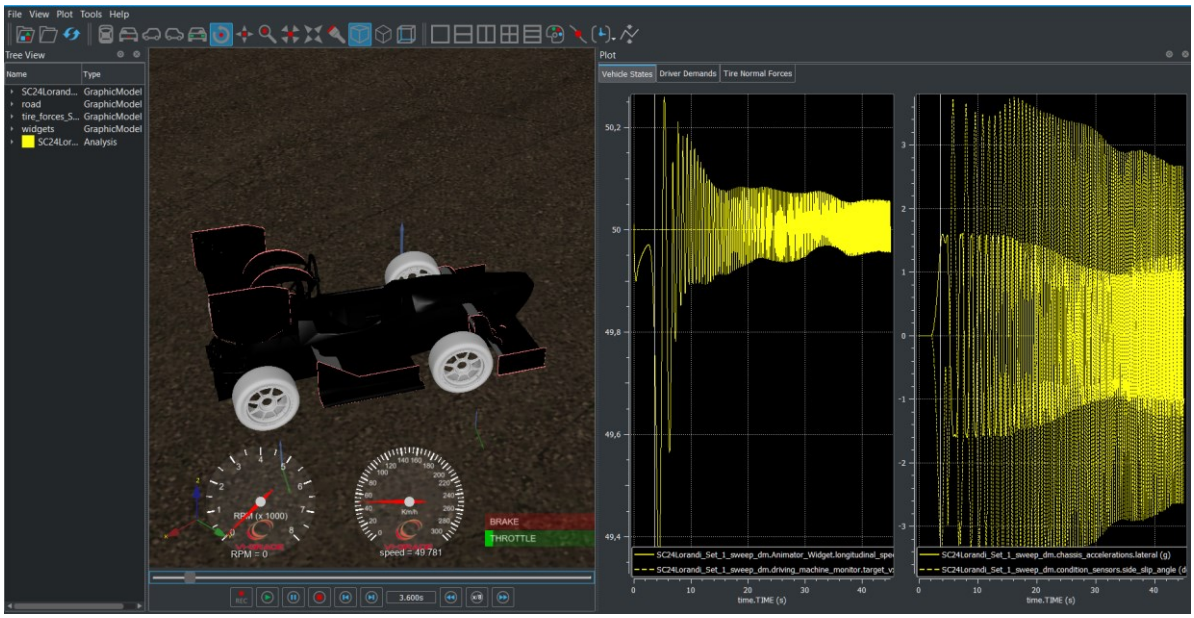


Figure 3.4 SC24 vehicle model in VI-CarRealTime simulation environment

The vehicle model used in this work was developed in VI-CarRealTime by Squadra Corse PoliTO. It represents the coupled dynamics of the chassis, suspension, tyres and powertrain using geometric, inertial and physical parameters consistent with SC24, as shown in Figure 3.4 [14].
The chassis is modelled as a rigid body with appropriate mass and inertia properties, while the suspension systems are represented through lookup tables reproducing the double wishbone pushrod layouts at both axles. The suspension model accounts for wheel travel, camber variation, and force transmission from the wheel to the chassis through the spring-damper units and anti-roll bars.
Tyre-road interaction is described with a Pacejka Magic Formula-based tyre model. While the model does not aim at an exact reproduction of absolute peak tyre forces under all tyre temperature conditions, it is considered to be sufficiently accurate to capture the main trends of lateral and longitudinal force generation within the range of slip, load, and camber values relevant to Formula Student events. This level of fidelity is adequate for the comparative analysis of suspension and damper setups conducted in this study.

The powertrain model reflects the all-wheel-drive electric architecture of the vehicle. Each wheel is driven by an independent electric motor, allowing individual torque application at each corner. For the purpose of model validation, the longitudinal dynamics are driven by torque signals measured during on-track testing, which already include the effects of traction control and torque vectoring strategies implemented on the real vehicle. This approach ensures consistency between the simulated and experimental operating conditions, while avoiding the need to replicate the full complexity of the real-time control logic within the offline simulation environment. Overall, the present VI-CarRealTime vehicle model provides a physically coherent representation of the vehicle dynamics of our prototype, with sufficient detail to analyse suspension behaviour, load transfer, and handling characteristics. Its structure makes it particularly suitable for systematic investigations of damper setup variations, which constitute the core of the present work.

3.4 MATLAB/Simulink Co-Simulation and Input Feeding

To enable a realistic excitation of the virtual vehicle model, a co-simulation framework was established between VI-CarRealTime and MATLAB/Simulink. This approach allows the direct use of input signals recorded during on-track testing, ensuring that the simulated vehicle is subjected to driving actions representative of real driving conditions, using an open-loop approach.
The co-simulation architecture is configured such that VI-CarRealTime solves the vehicle dynamics equations, while MATLAB/Simulink handles the input signal processing and delivery.
Steering angle and wheel torque signals are supplied to the virtual model as time-varying inputs. Steering and braking inputs correspond to driver commands, while longitudinal wheel torques include both traction and regenerative braking components and are applied directly at the wheel level.
The input signals used in the simulations are taken directly from recorded telemetry data and are used in their raw form, without additional filtering or artificial shaping. This choice was made to preserve the original characteristics of the driver inputs and to avoid introducing assumptions that could alter the dynamic response of the model. The resulting simulations therefore aim to reproduce the same excitation conditions experienced by the real vehicle during the test sessions.
In the validation phase, the measured wheel torque signals already processed by the vehicle's traction control and torque vectoring systems are imposed on the virtual model, effectively bypassing the detailed powertrain control logic. This strategy ensures coherence between experimental and simulated longitudinal dynamics and isolates the effects of suspension and chassis behaviour, which are the primary focus of the present study. In subsequent offline simulations dedicated to damper setup comparison, simplified powertrain assumptions are adopted, as the detailed replication of the real-time control architecture is beyond the scope of this work.
The co-simulation framework provides a robust and flexible tool to replay real driving manoeuvres in a virtual environment.

3.5 Track-Test Instrumentation

The onboard acquisition system includes many sensors. Only the devices directly relevant to the signals used in this study are described below.

3.5.1 MicroAutoBox II



Figure 3.5 dSPACE MicroAutoBox II used for onboard acquisition and control (source: dSPACE [15])

The vehicle control unit is a dSPACE MicroAutoBox II 1401/1511. It acquires the signals used in this work and runs control functions developed in MATLAB/Simulink and compiled for real-time execution, as shown in Figure 3.5 [15].

3.5.2 IMU - SBG Ellipse-N



Figure 3.6 SBG Systems Ellipse-N inertial navigation system (source: SBG Systems [16])

This inertial measurement unit provides data regarding: [16]

- Accelerations
- Roll/Pitch
- GPS Position
- Azimuth

The sensor is fixed to the chassis in the middle of the front coilovers on a surface which should be as flat as possible when the car is on the ground with the driver onboard, as prescribed for the internal GNSS receiver.

3.5.3 Vehicle Sideslip-Angle Sensor - Kistler CORREVIT S-Motion Standard

The Kistler CORREVIT S-Motion Standard, as shown in Figure 3.7 [19], provides direct optical measurements of vehicle sideslip angle and longitudinal and lateral velocity.
The sensor was installed at the rear of the vehicle, aligned vertically with respect to the ground and positioned on the longitudinal symmetry plane. Its longitudinal distance from the vehicle centre of gravity was known, allowing the measured quantities to be referred to the CoG. The installation orientation was selected according to the manufacturer's specifications.
Sensor configuration was performed through the dedicated KiCenter software. The device provides programmable and standardised output signals and interfaces, enabling direct connection to a PC or to the vehicle data acquisition system. The following quantities can be measured and recorded:

- Travelled distance;
- longitudinal and lateral velocity components;
- vehicle sideslip angle;
- accelerations and angular rates;
- GPS position and UTC time
- pitch and roll angles.



Figure 3.7 Kistler CORREVIT S-Motion Standard (source: Kistler [19])

3.5.4 Steering-Angle Sensor

The RLS RM08 is a compact, non-contact rotary magnetic encoder used to measure steering angle. Its sealed two-part construction avoids bearings and dynamic seals and is suitable for the limited installation space available on the prototype, as shown in Figure 3.8 [17].



Figure 3.8 RLS RM08 magnetic steering-angle encoder (source: RLS [17])

3.6 On-Track Telemetry and Validation Manoeuvres

The validation of the virtual vehicle model is based on telemetry data acquired during on-track testing of the Formula Student prototype. The selected datasets are representative of typical driving conditions encountered during Autocross and Endurance events, characterised by combined lateral and longitudinal loading, rapid transients, and frequent transitions between steady-state and dynamic manoeuvres. The recorded telemetry includes both driver inputs and vehicle response signals. In particular, the following channels are considered relevant for the validation of the virtual vehicle model:

- longitudinal acceleration a_x
- lateral acceleration a_y
- yaw rate
- vehicle sideslip angle β
- vehicle speed
- wheel rotational speeds
- wheel torque signals at each corner
- steering input

These signals were selected because they directly reflect the vehicle's global dynamic behaviour and its response to driver inputs and are therefore suitable for assessing the accuracy of the virtual model in reproducing real-world conditions.

The validation manoeuvres were not based on complete laps, but on selected dynamic tests specifically aimed at assessing the lateral behaviour of the vehicle model.
The manoeuvres selected for the experimental assessment consisted of slalom tests, double lane changes, and steering-frequency sweeps, all performed at the Squadra Corse test track at the Cerrina racetrack. Since the tests were conducted on an existing track rather than on a dedicated proving ground, the available space constrained the execution of highly standardised manoeuvres. In sweep-steer tests requiring long straight sections or large run-off areas could not be performed under sufficiently safe and repeatable conditions.
This choice reflects the objective of the validation process, which was not to reproduce the full vehicle behaviour in every possible operating condition, but to verify that the virtual model could capture the main lateral dynamic response of the prototype.
Particular attention was given to quantities such as lateral acceleration, yaw rate and sideslip angle, since these responses are directly related to the handling behaviour of the vehicle and are significantly influenced by suspension and damper characteristics.
Longitudinal and strongly combined manoeuvres were not treated as primary validation cases, since the scope of the present work is focused on the influence of damper settings on lateral dynamics. Therefore, braking-dominated or traction-dominated phases were not used as main criteria for model validation, except where their influence was unavoidable within the selected manoeuvres.
All telemetry signals used for validation were taken directly from the on-board data acquisition system. The comparison between simulated and experimental data was performed using equivalent input and output time histories, in order to assess the capability of the virtual vehicle to reproduce the measured response under realistic lateral excitation conditions.

3.7 Model-to-Track Correlation and Discussion

The correlation between the virtual vehicle model and the experimental data is assessed through a direct comparison of simulated and measured time histories for the selected signals. The analysis focuses on the ability of the model to reproduce the overall trends, peak values, and transient behaviour observed in the real vehicle, rather than on achieving a perfect point-by-point match.
All manoeuvres were performed during the same test session and with an unchanged wheel-alignment setup, in order to minimise variations in tyre-road grip and reduce the influence of environmental and operating conditions. Only tests characterised by limited differences in tyre temperature were considered in the analysis, while the first runs were discarded because they were affected by the initial tyre warm-up phase. Traction Control was kept active throughout the tests for safety reasons.

3.7.1 Frequency Sweep

Figures 3.9-3.12 compare the measured and simulated responses during the steering-frequency sweep for the main validation quantities.
The manoeuvre was intended as a steering-frequency sweep at an approximately constant speed of 50 km/h, obtained by limiting the power delivered by the traction battery.
The sine-sweep steering test is commonly employed for vehicle-model validation, as it allows the dynamic response of the vehicle to be evaluated over a range of increasing steering-input frequencies.

The tests did not provide sufficiently reliable results for the direct estimation of the vehicle transfer functions. The main limitation was the restricted width and length of the available straight sections of the racetrack. Consequently, the acquired signals contained an insufficient amount of data at each excitation frequency, while the steering frequency varied too rapidly to obtain reliable frequency-response estimates.
A further limitation was associated with the manual execution of the steering input. At higher excitation frequencies, the driver could not accurately reproduce the desired sinusoidal profile, particularly because of the limited track width and the risk of vehicle instability. Corrective counter-steering actions were therefore occasionally introduced, altering the intended input signal. These effects became increasingly significant as the vehicle speed increased.
Although the tests were not suitable for a rigorous experimental identification of the vehicle transfer functions, they were retained as validation manoeuvres for the virtual vehicle model. Their continuously varying steering input provided a useful excitation for assessing the model response over different frequencies and operating conditions, particularly in terms of lateral acceleration, yaw rate and sideslip angle.

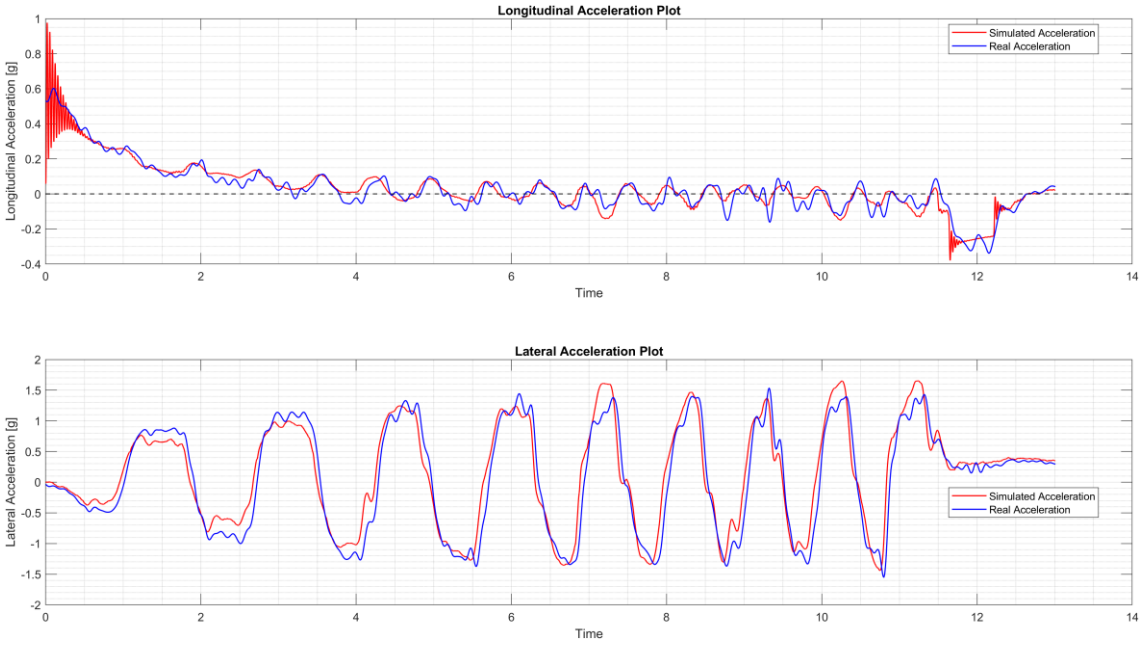


Figure 3.9 Measured and simulated longitudinal and lateral acceleration during the steering-frequency sweep

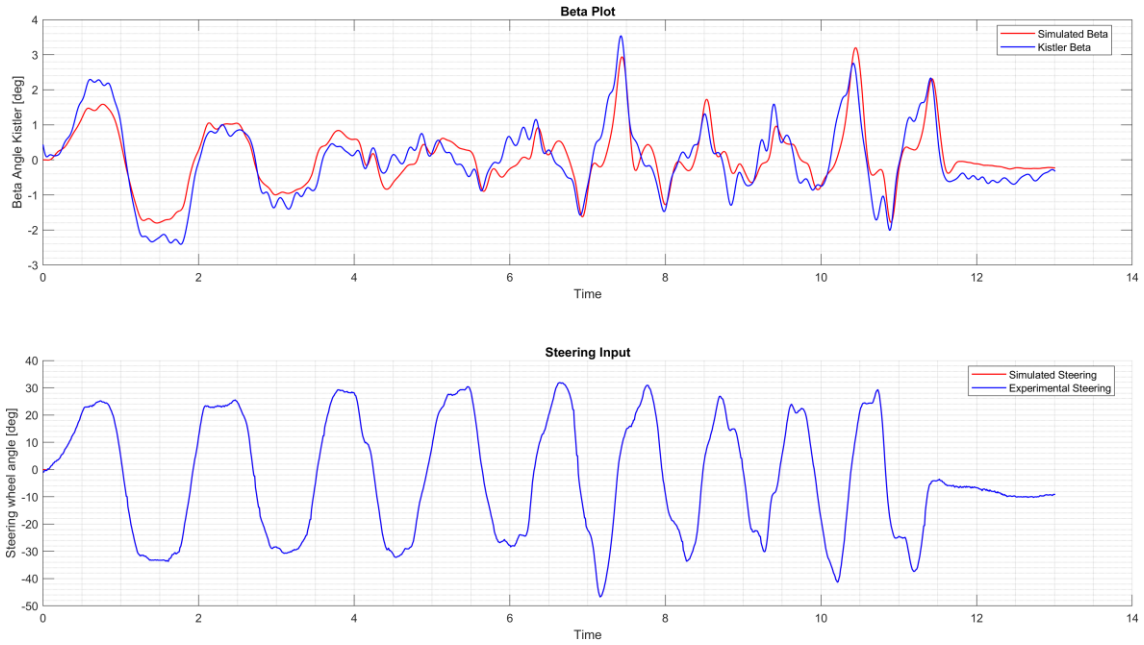


Figure 3.10 Measured and simulated sideslip angle and steering-wheel angle during the steering-frequency sweep

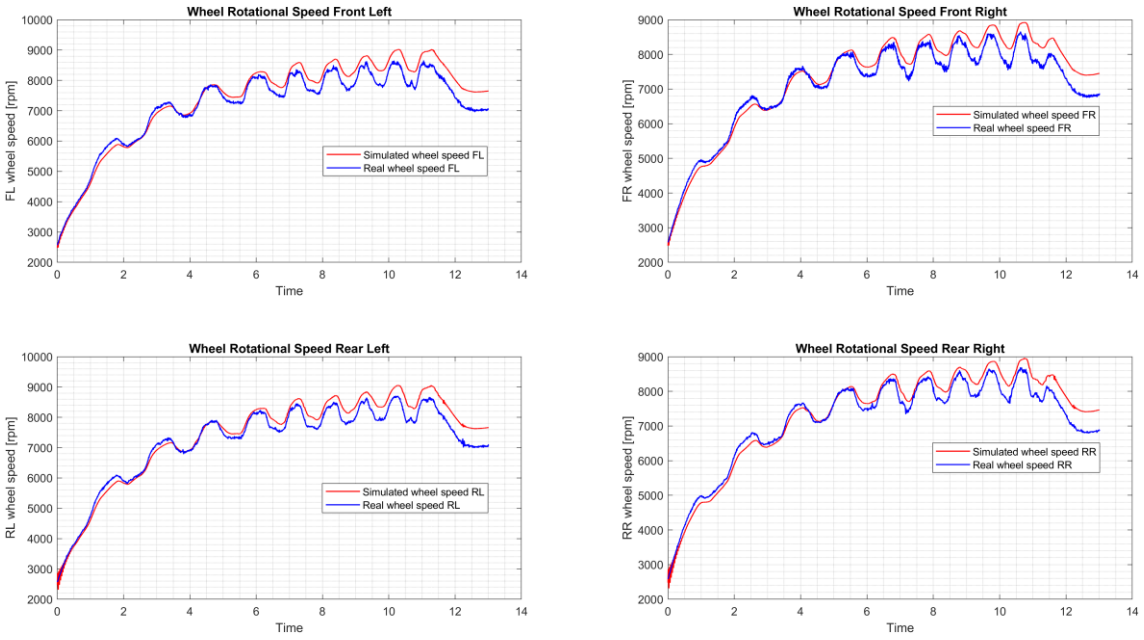


Figure 3.11 Measured and simulated wheel speeds during the steering-frequency sweep

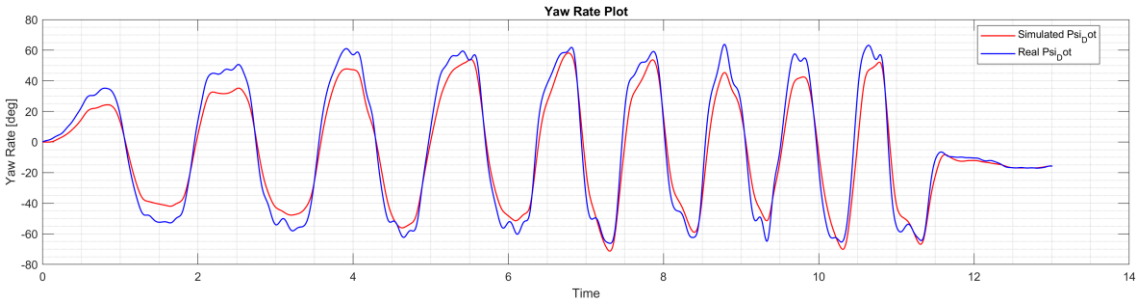


Figure 3.12 Measured and simulated yaw rate and lateral acceleration during the steering-frequency sweep

3.7.2 Double Lane Change

The double lane change layout was characterised by a lane width of approximately 3.5 m, a gate width of about 6 m, and a longitudinal spacing of approximately 7 m between consecutive gates.

The power available to the driver was limited to approximately 12 kW, with no additional wheel-torque limit. The driver accelerated before the first lane change and completed the manoeuvre at full throttle. The corresponding comparisons are reported in Figures 3.13-3.16.

The power level used for the test was determined through an iterative trial-and-error procedure. Starting from an initial power setting, the limit was progressively increased whenever the driver successfully completed the manoeuvre. This process continued until the test could no longer be performed consistently and safely. The selected operating condition therefore represented a demanding, but still repeatable, execution of the double lane change. Maximum reached speed was 55 kph.

As for the frequency sweep tests, all double lane change manoeuvres were performed during the same test session and without modifying the wheel-alignment setup, in order to minimise variations in vehicle behaviour caused by setup or environmental changes. Tyre temperatures were measured after each run and ranged between 22 °C and 26 °C, which is quite cold and far away from optimal operating conditions.

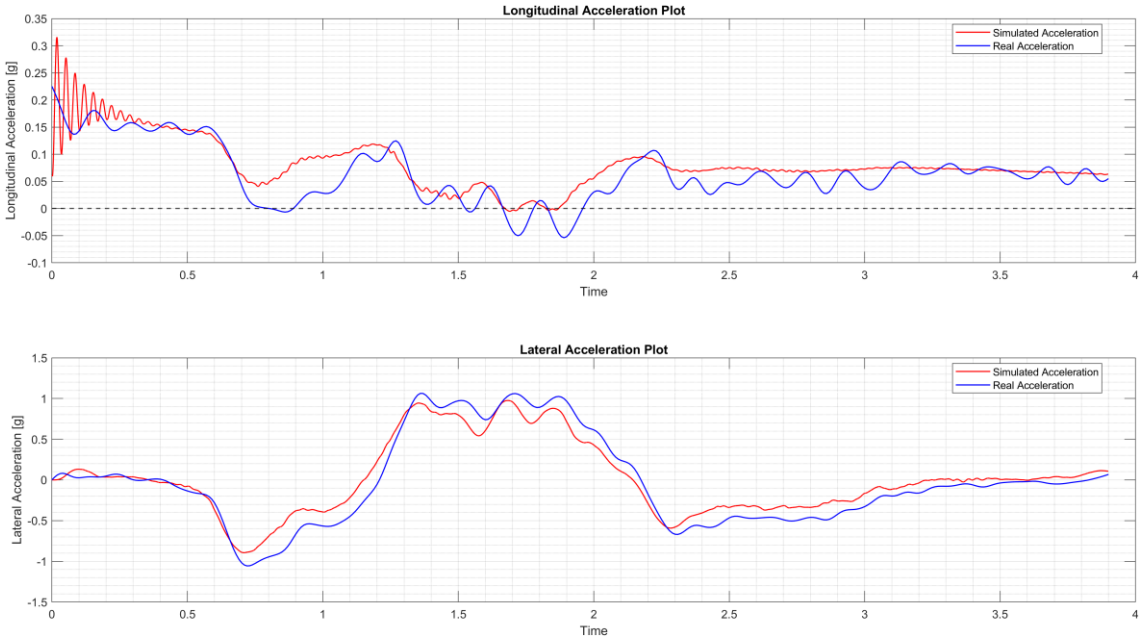


Figure 3.13 Measured and simulated longitudinal and lateral acceleration during the double lane change

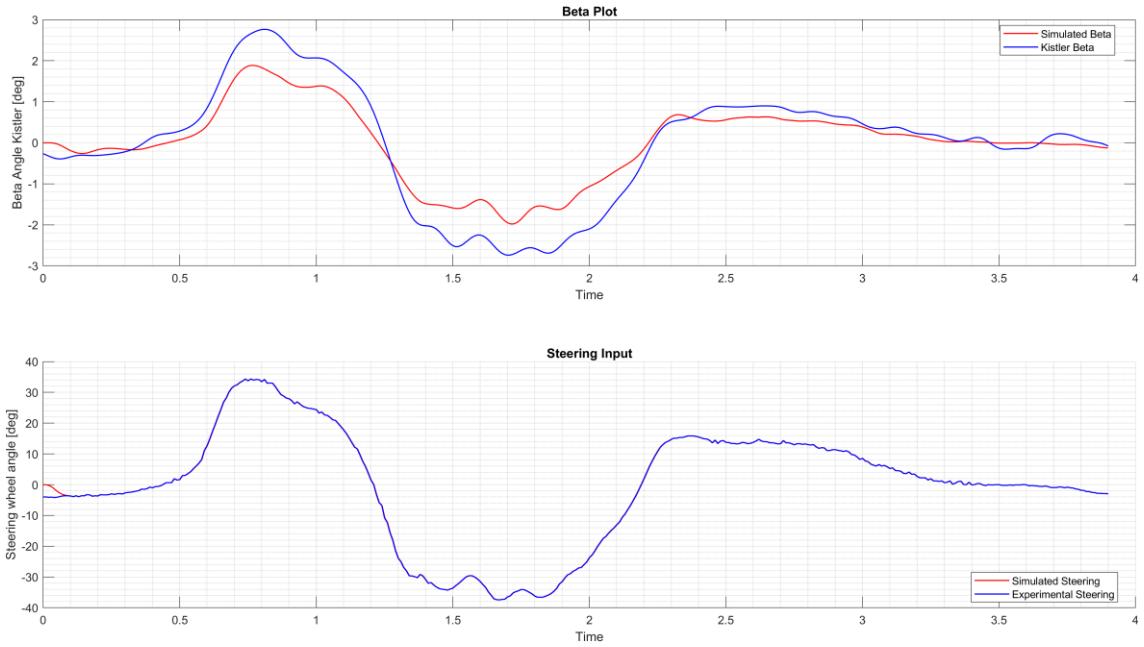


Figure 3.14 Measured and simulated yaw rate and sideslip angle during the double lane change

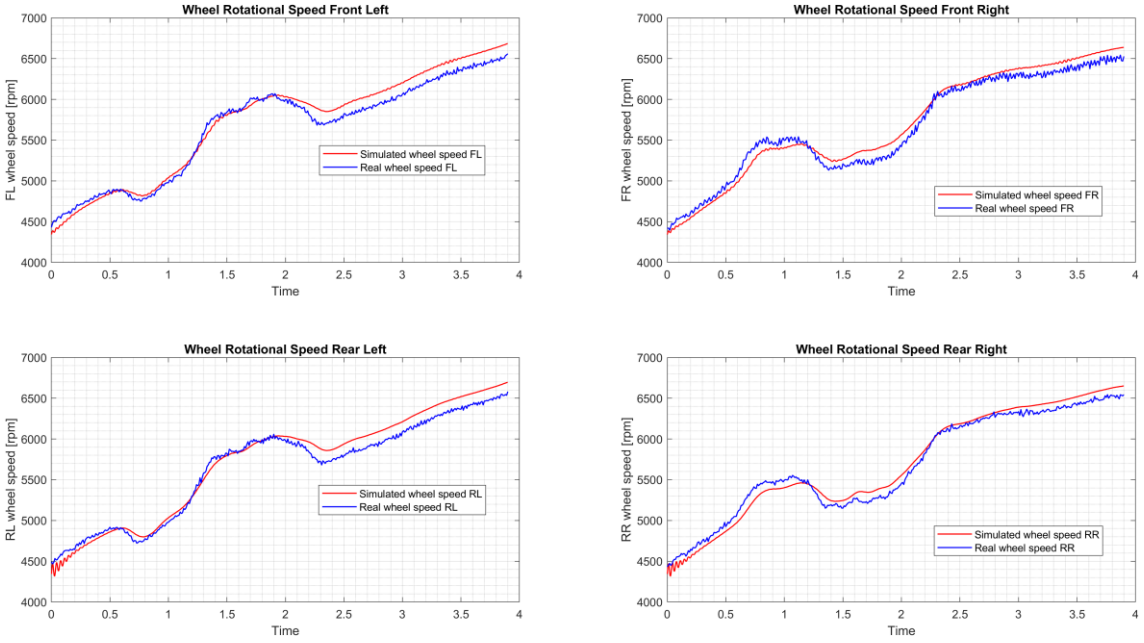


Figure 3.15 Measured and simulated wheel speeds during the double lane change

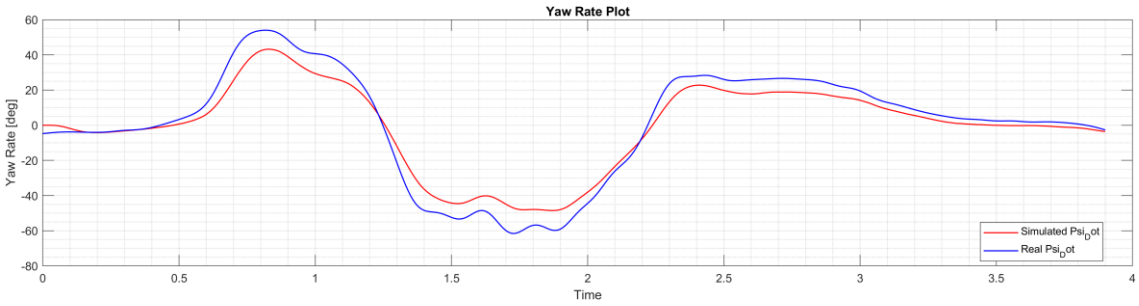


Figure 3.16 Measured and simulated vehicle speed and steering-wheel angle during the double lane change

3.7.3 Slalom

The slalom has 8 m between consecutive gates, as in Formula Student Germany Rules [1]. The vehicle approached under braking, completed the cones with combined steering and throttle, and accelerated after the final gate. Figures 3.17-3.20 compare the measured and simulated responses.

Tyre temperatures were measured at the end of each manoeuvre and ranged between 23 °C and 32 °C. These values are below the optimal operating range of the tyres and therefore represent a particularly demanding condition for the vehicle. Nevertheless, they are representative of Formula Student competition use, where the limited duration of the dynamic events generally prevents the tyres from reaching and maintaining their ideal working temperature.

In the time series plot of Figures 3.17-3.20 is appreciable that the yaw rate measured and the simulated one are clearly overlapping, both for maximum and minimum values during the maneuver and for the dynamic behaviour.

The measured longitudinal-acceleration signal shows a few small oscillations relative to the simulated response, as expected because of measurement noise. The vehicle sideslip-angle signals overlap slightly less closely, but the real and simulated vehicles still show similar behaviour in the main peaks and overall trend.

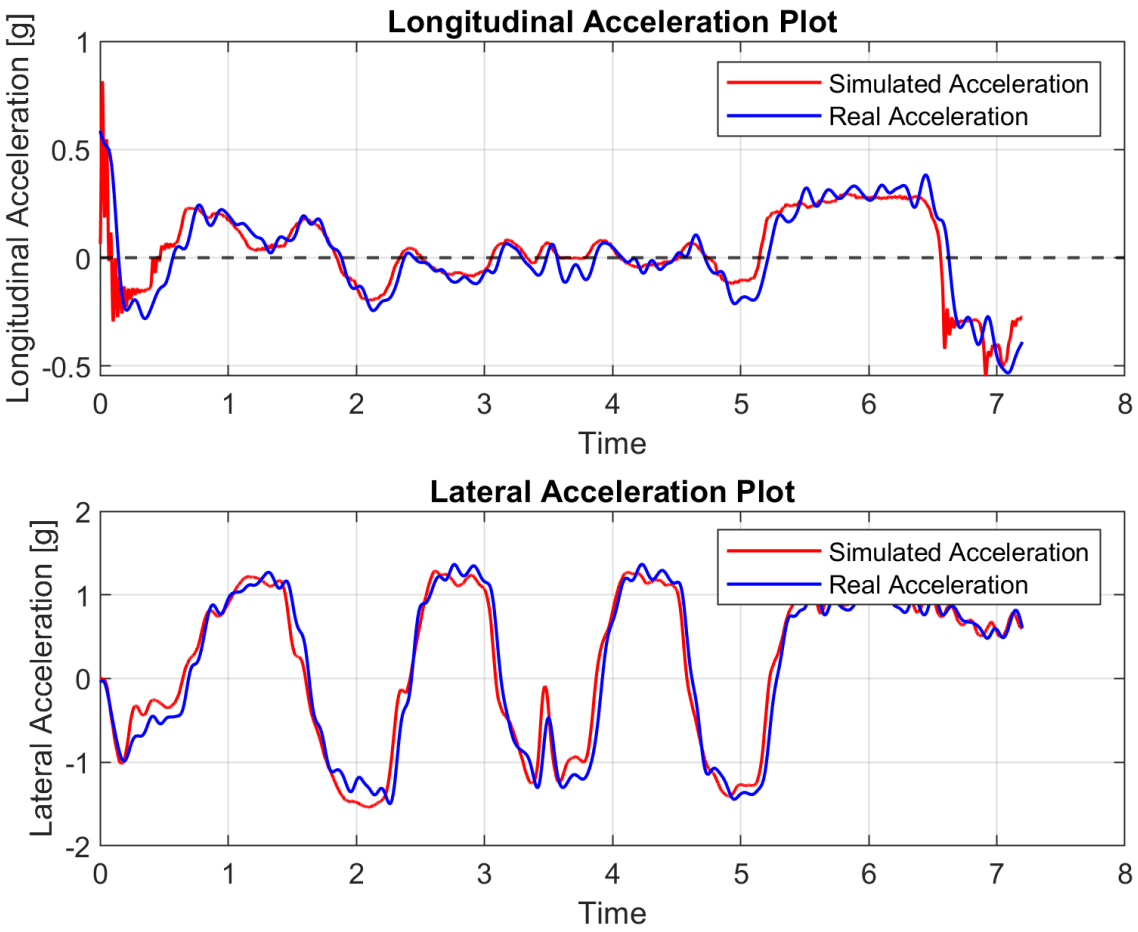


Figure 3.17 Measured and simulated longitudinal and lateral acceleration during the slalom

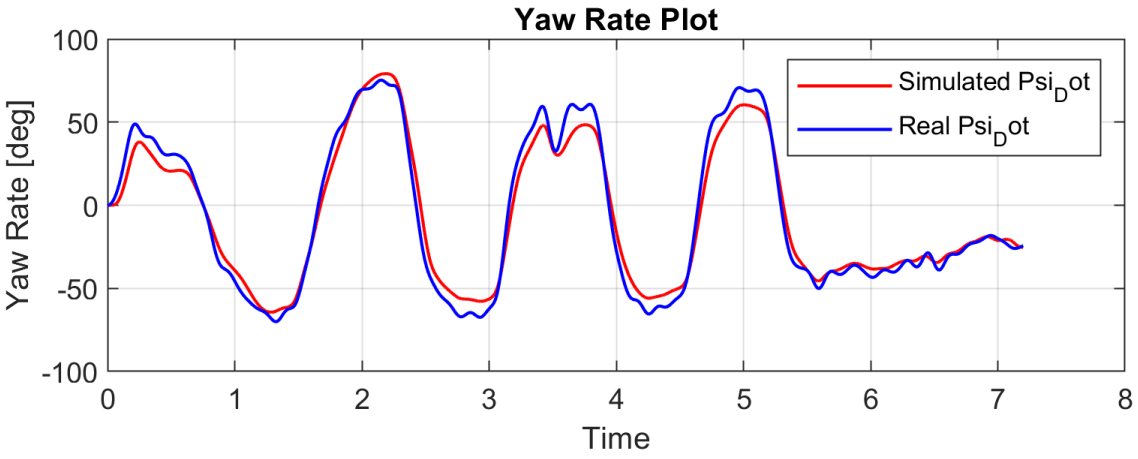


Figure 3.18 Measured and simulated yaw rate and lateral acceleration during the slalom

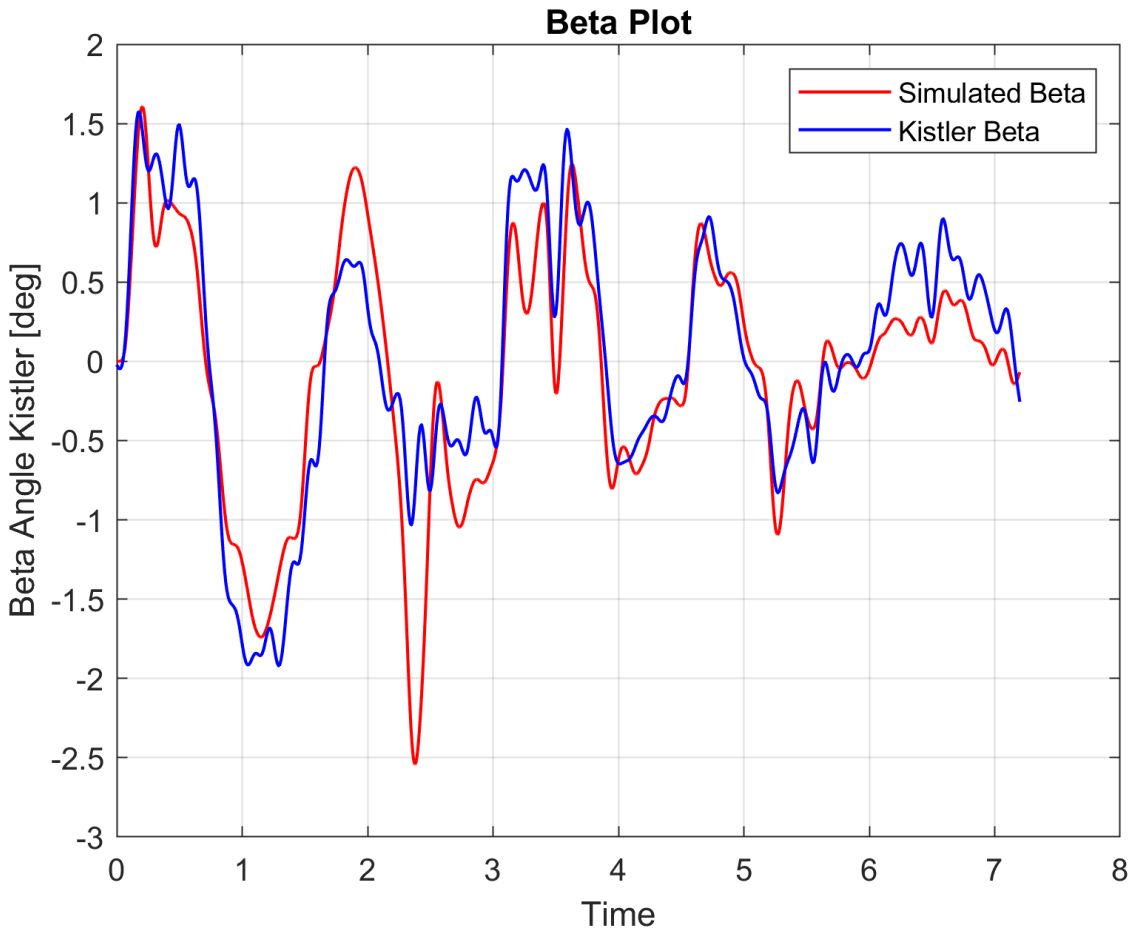


Figure 3.19 Measured and simulated sideslip angle during the slalom

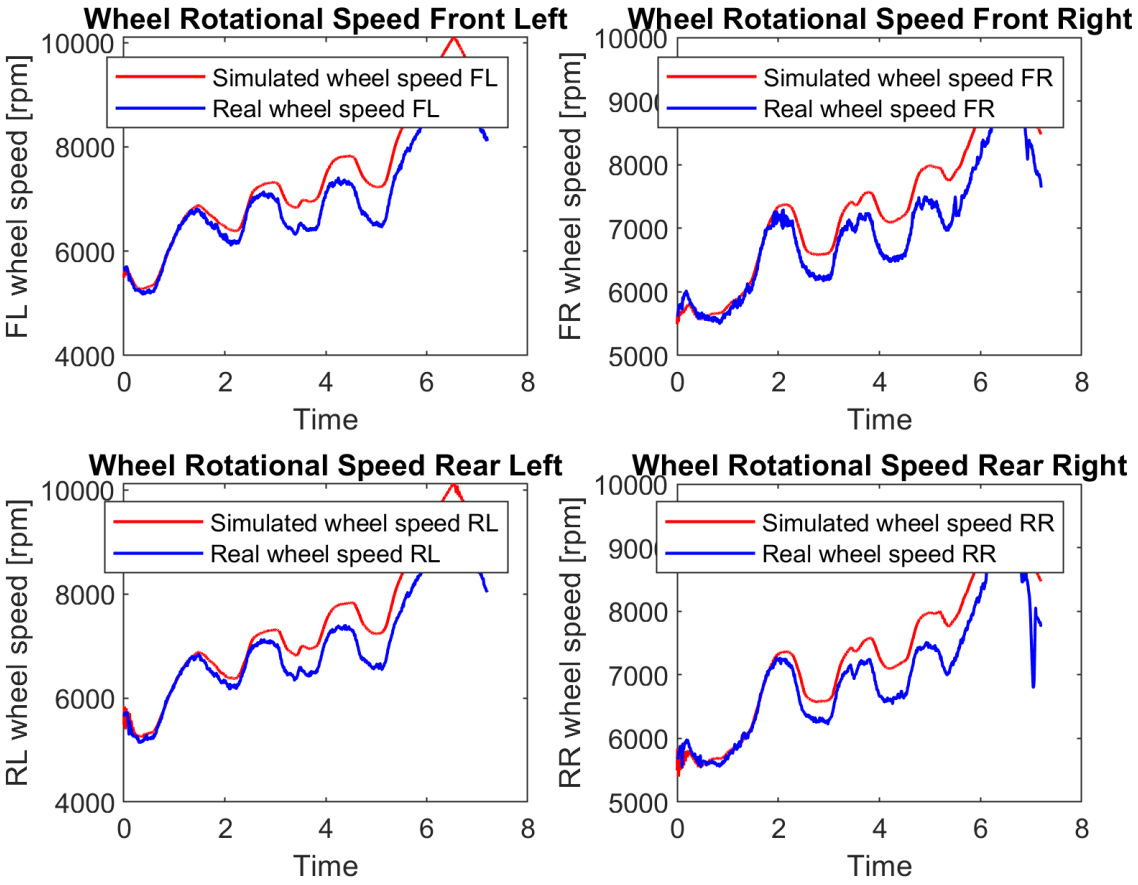


Figure 3.20 Measured and simulated wheel speeds during the slalom

3.8 Validation Comments

Across the three manoeuvres, lateral and longitudinal acceleration show a satisfactory agreement in amplitude, change rate and trend evolution. Simulated yaw rate and sideslip angle also reproduce the main measured trends. The comparison therefore indicates that the model captures the dominant mechanisms governing vehicle rotation and lateral balance within the tested operating range.

Wheel rotational speeds and vehicle speed are also compared to assess the coherence of longitudinal dynamics. The use of measured wheel torque inputs in the validation phase contributes to a consistent reproduction of traction and regenerative braking effects, allowing the suspension and chassis response to be analysed independently from powertrain control uncertainties.

Some discrepancies remain, particularly in peak vehicle sideslip. They are consistent with limitations in the tyre-model parametrisation and with the sensitivity of the real tyres to temperature and inflation pressure.

Most runs were performed at low tyre temperature and therefore under reduced-grip conditions.

Additionally, the modelling of the hydraulic braking system is simplified, as brake pressure measurements are limited to the master cylinder and rear brake forces are inferred through brake bias assumptions. These aspects introduce uncertainties in the reproduction of pure braking events and combined braking-cornering phases.

Despite these limitations, the correlation is considered adequate for screening damper configurations under consistent simulated conditions. The validation supports the model's main lateral and longitudinal trends; it does not independently prove the accuracy of every predicted damper sensitivity or wheel-lift event. Those results must still be confirmed on track.
On this basis, the model is used in the following chapters to compare force-velocity characteristics under repeatable conditions while maintaining a clear link with the measured behaviour of SC24.

4 Experimental Characterisation of the Dampers

4.1 Damper Characterisation and Supplied Damper Data

This chapter describes the experimental characterisation of the passive hydraulic dampers installed on the Formula Student prototype. The purpose of this activity is not to provide a purely descriptive overview of dynamometer plots and the methodology to obtain them, but to establish a compact and physically meaningful representation of the available damper configurations, which will be used to guide the setup selection and optimisation process in the subsequent chapter.
Given the large number of possible adjustment combinations offered by the four-way dampers (independent low-speed and high-speed settings in compression and rebound), an exhaustive trial-and-error exploration is impractical. Therefore, the damper characterisation is used to:

- Quantify how the force-velocity behaviour changes with the adjustment clicks,
- Identify the critical damping percentages along the curve (low-speed vs high-speed, compression vs rebound)
- Support the definition of a limited number of representative setups to be tested in the virtual environment.

Ultimately, the damper setup optimisation strategy adopted in this thesis is built upon the link between measured damper force-velocity characteristics and vehicle-level phenomena such as vertical load transients, wheel contact consistency, and handling balance under combined manoeuvres.
The force-velocity characteristics used in this work were provided by the damper supplier and were obtained from dynamometer measurements. The dataset contained several curves corresponding to different damper adjustment configurations, covering both compression and rebound over a shaft velocity range of approximately 0-300 mm/s.
Detailed information concerning the dynamometer test procedure, the internal damper configuration, and the rationale adopted by the supplier to define the different click combinations was not available. Consequently, the present work does not attempt to reconstruct the individual influence of the low-speed and high-speed compression and rebound adjusters. The supplied curves are instead treated directly as candidate force–velocity maps for implementation in the vehicle model.
This distinction is relevant because the objective of the present activity was not to experimentally redesign or fully characterise the damper, but to select a limited number of existing characteristics and evaluate their effect at vehicle level.

4.2 Damper Hardware and Test Data Overview

The car uses four-way adjustable passive hydraulic dampers mounted coaxially with the springs in a pushrod layout suspension. Separate low-speed and high-speed compression and rebound adjustments are available. The same hardware is used at both axles, although axle-specific settings may be adopted on track to account for the different loads and driver feedback.
Experimental damper data were provided by the damper supplier in the form of force-velocity characteristics obtained from dynamometer testing. The dataset includes sweeps where only one adjustment is varied while the others are kept fixed, as well as combined sweeps where low-speed and high-speed settings are changed simultaneously.

Each characteristic was supplied as discrete force and shaft-velocity values. Compression and rebound are contained in the same lookup table, with negative velocity denoting compression and positive velocity denoting rebound according to the sign convention used in the VI-CarRealTime model.
The supplied points were converted into consistent SI units and directly implemented through one-dimensional lookup tables. Interpolation between the measured points was embedded in VI-CarRealTime software to obtain a continuous force output over the complete velocity range. No additional modification of the force values was introduced. Only mean force-velocity characteristics were available. Hysteresis, friction, temperature sensitivity and frequency-dependent behaviour could not be identified separately, so the implemented maps are a static representation rather than a complete dynamic damper model.

The force-velocity curves exhibit distinct regions that can be associated with different operating regimes. At low shaft velocities, the slope of the curve reflects the behaviour of the low-speed damping circuits, which primarily influence vehicle body motions and load transfer dynamics. At higher velocities, changes in slope indicate the activation of high-speed damping mechanisms, which govern the response to road irregularities, kerbs, and sharp suspension inputs.

4.3 Preliminary Screening Criterion

Because the supplier dataset contained many candidate characteristics, a preliminary screening criterion was introduced before the vehicle-level simulations. The purpose was not to identify an optimum, but to remove curves with clearly unsuitable low-speed force levels. The comparison used the equivalent damping generated at a reference shaft velocity of approximately 20 mm/s. The full-lap damper-velocity and roll-rate distributions supporting this choice are shown in Figure 4.1.

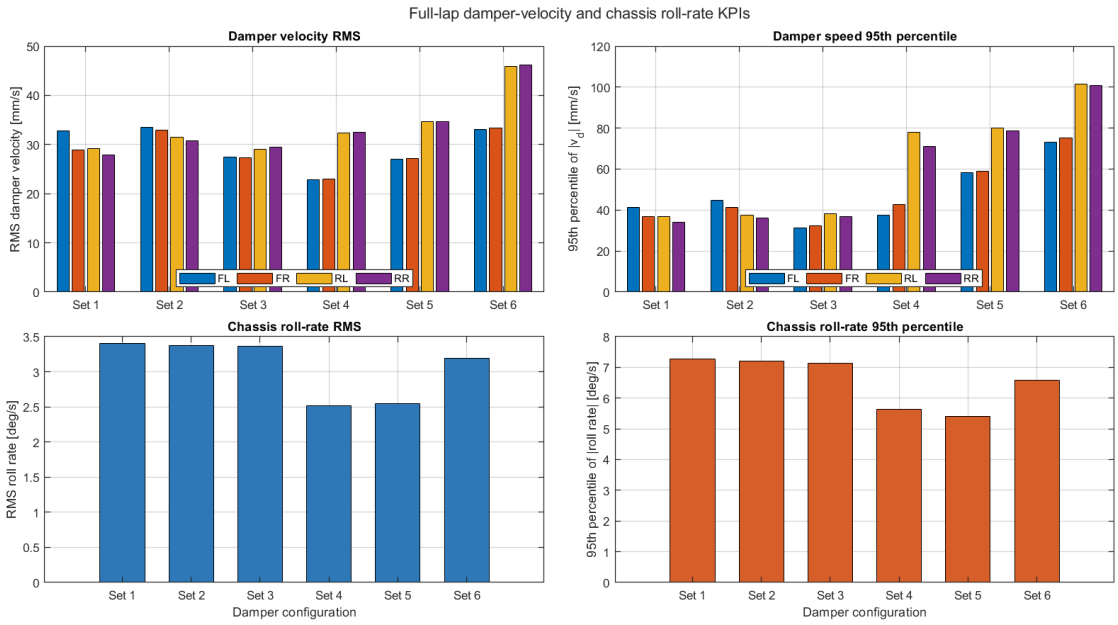


Figure 4.1 Damper-velocity and roll-rate distributions over the reference lap

For a nonlinear force-velocity characteristic, and thus for each compression and rebound branch, an equivalent secant damping coefficient can be defined at the selected reference velocity as

$$c_{\mathrm{eq}}(v_{\mathrm{ref}}) = \frac{\mid F_d(v_{\mathrm{ref}}) \mid}{\mid v_{\mathrm{ref}} \mid}$$

where $F_d$is the damper force and v_{ref} is the reference shaft velocity. The damper coefficient was then converted into an equivalent wheel-side coefficient using the local suspension installation ratio, so that it could be compared with the critical damping coefficient calculated at the same wheel coordinate.
The critical damping coefficient was obtained from a linear one-degree-of-freedom approximation of the suspension corner:

$$c_{\mathrm{cr}} = 2\sqrt{k_{\mathrm{eq}} m_{\mathrm{eq}}}$$

The equivalent damping ratio was then expressed as

$$\zeta_{\mathrm{eq}}(v_{\mathrm{ref}}) = \frac{c_{\mathrm{eq}}(v_{\mathrm{ref}})}{c_{\mathrm{cr}}}$$

with all quantities referred to the same single wheel corner.
A secant coefficient was preferred to a local tangent coefficient for this preliminary comparison. The tangent value is strongly affected by the spacing of the measured velocity breakpoints and may therefore vary considerably depending on the points used to estimate the local slope. Conversely, the secant coefficient directly represents the force level generated at the selected operating point and provides a more robust indicator for comparing a large number of curves.
The critical coefficient is obtained from a linearised ride model containing only the sprung mass and the wheel-side spring stiffness. It therefore neglects tyre compliance, unsprung-mass dynamics and the contribution of the anti-roll bars. Furthermore, the dampers are nonlinear and asymmetric, meaning that their equivalent damping changes with shaft velocity and direction. Consequently, a value greater than (100%) does not necessarily imply that the complete vehicle response is overdamped.
Curves producing equivalent damping levels several times greater than the critical reference were excluded from the initial simulation set. Six characteristics closer to the selected range were retained. This step reduced the dataset.
Characteristics with very low equivalent low-speed damping were also excluded. Because SC24 has no dedicated roll damper, the conventional wheel dampers must control the roll transient. The anti-roll bars act in parallel with the ride springs in roll, increasing the equivalent roll stiffness and the corresponding critical roll damping coefficient.

4.4 Selected Configurations

The six selected characteristics were implemented without further modification because the click combinations required to generate intermediate curves were not known. The same curve was applied at all four corners. Table 4.1 reports different equivalent front and rear damping ratios because the sprung masses, wheel rates and installation ratios differ slightly between the axles.
The configurations are labelled Set 1 to Set 6; the numbering is arbitrary and identifies only the force-velocity curve shown in Figure 4.2.
The equivalent damping ratio was used only for screening while the actual comparison is based on the reduced-order responses in this chapter and on the complete-vehicle simulations in Chapter 5.

Table 4.1 Low-speed equivalent damping ratios for the six selected sets

Set	Axle	Compression % Critical Damping	Rebound % Critical Damping
1	Front	144.1	107.7
1	Rear	123.1	92.1
2	Front	125.9	67.5
2	Rear	107.6	57.7
3	Front	58.4	31.1
3	Rear	49.9	26.6
4	Front	318	231
4	Rear	271.8	197.4
5	Front	76.6	35
5	Rear	65.4	29.9
6	Front	42.8	10.4
6	Rear	36.6	8.9

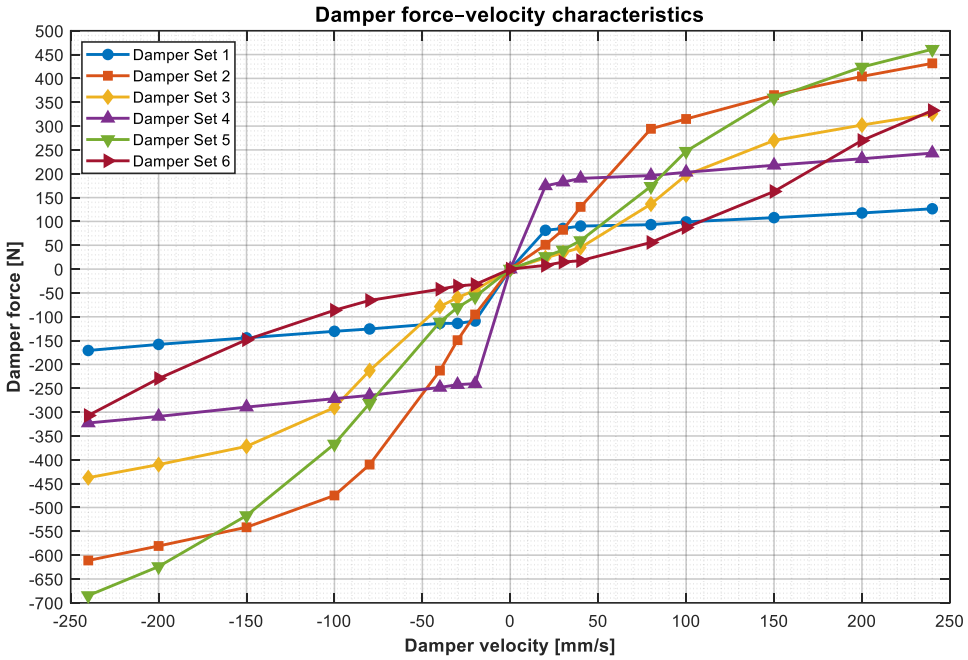


Figure 4.2 Selected damper force-velocity characteristics implemented in the vehicle model

4.5 Reduced-Order Dynamic Assessment and Link to Damper Optimisation

The equivalent damping ratio evaluated at a chosen rod velocity provides only a preliminary indication of the force level generated by each curve. It does not describe how the nonlinear damper interacts with the sprung mass, unsprung mass, tyres and anti-roll bars, nor does it identify the frequency ranges in which the differences between the configurations become relevant. For this reason, the six retained sets were also compared using simplified vertical and roll models before their evaluation in the complete vehicle model.

4.5.1 Vertical Response

The front and rear axles were analysed separately using two-degree-of-freedom quarter car model.
A prescribed road-displacement step of 25 mm was applied at the contact patches. The outputs selected for comparison were the vertical displacement of the sprung mass and the variation of the vertical tyre force ΔF_z. The former provides a first-order indication of the ability of the suspension to control the vertical motion of the vehicle platform, which is particularly relevant for a vehicle with aerodynamic devices. The latter describes the transient variation of the load transmitted through the tyre and is therefore

directly related to road holding and to the availability of longitudinal and lateral tyre forces [2,5,8,12].
Sprung-mass acceleration, a common ride-comfort metric, was not adopted as a primary output because passenger comfort is outside the scope of this work. Unsprung-mass displacement was retained as an internal state of the model.
The step responses in Figure 4.3 compare peak vertical-load variation, overshoot and settling behaviour. Because the spring and tyre properties are unchanged, all sets converge to the same static condition; the differences are caused by the transient nonlinear damper forces.

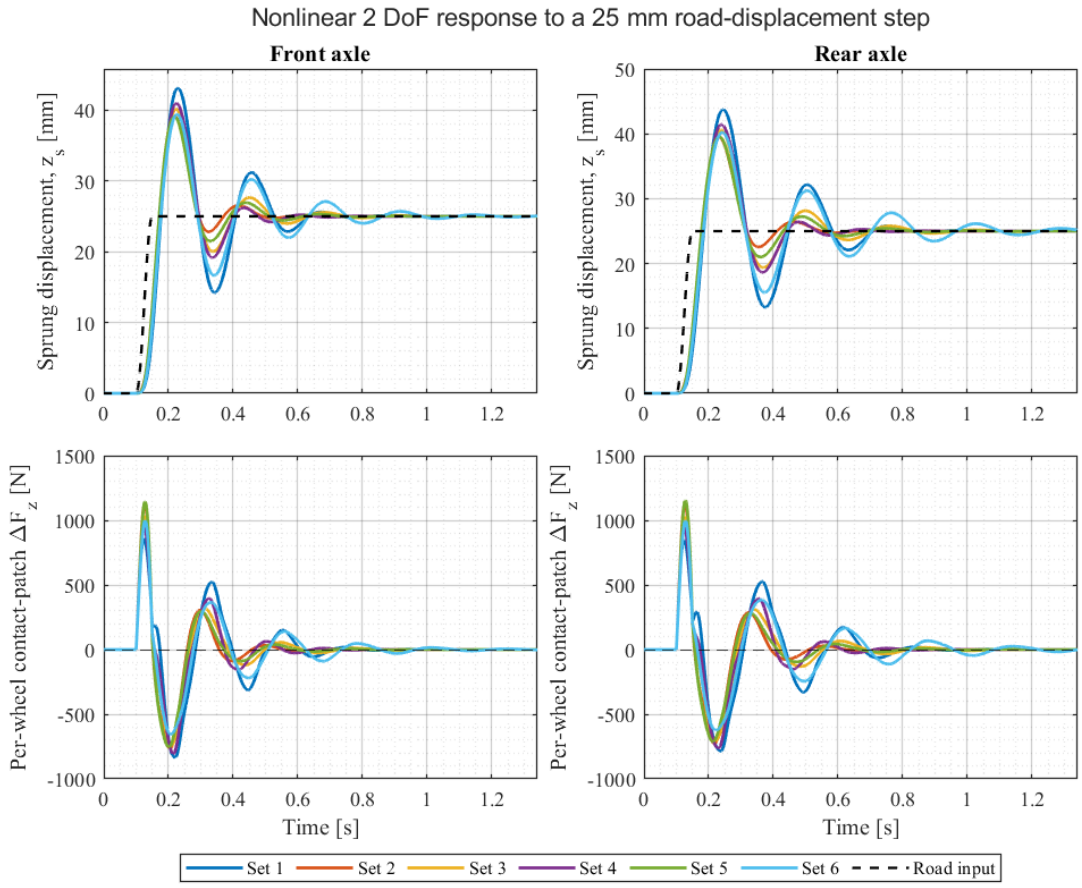


Figure 4.3 Nonlinear quarter-car step response for the selected damper characteristics

The same models were then excited by a logarithmic swept-sine purely vertical road displacement. The investigated frequency interval extended from the low-frequency sprung-mass mode to slightly above the higher-frequency unsprung-mass or wheel-hop zone.

The resulting functions describe the ratios

$$\frac{Z_s(f)}{Z_r(f)} \text{ and } \frac{\Delta F_z(f)}{Z_r(f)}$$

where Z_r is the imposed road displacement and Z_s is the sprung-mass displacement. These outputs respectively describe the transmission of the road input to the vehicle platform and the amplification of the contact-patch load variation.

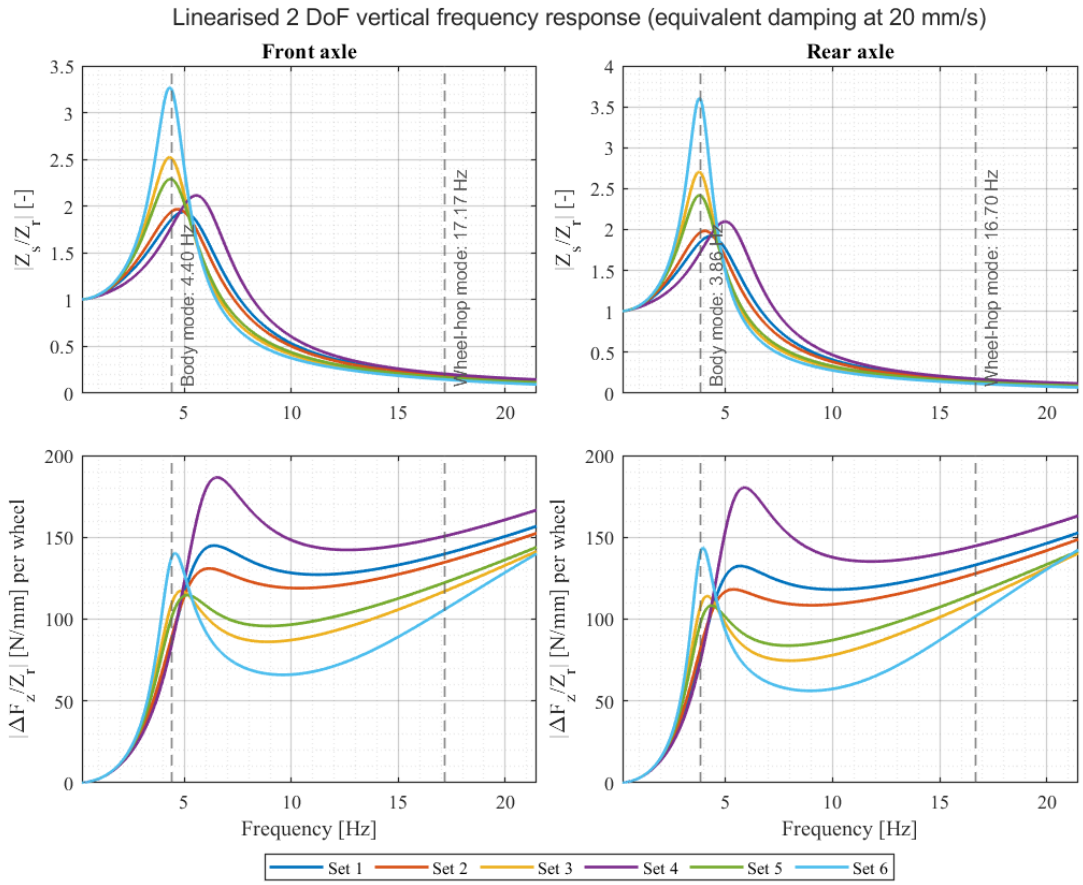


Figure 4.4 Linearised two-degree-of-freedom vertical frequency response of the selected configurations

Figure 4.3 shows that Set 6 is clearly the least-damped configuration. Together with Set 1, it also produces one of the longest disturbances of the sprung-mass displacement and vertical-load variation, which is undesirable. Set 2 provides the best compromise between the first-peak amplitude and the damping of subsequent oscillations.
A different conclusion can be drawn from Figure 4.4, which shows that Sets 1, 2 and 4 produce larger contact-patch vertical-load variations above approximately 5 Hz. In the simplified model, these configurations transmit high-frequency road disturbances more strongly to the tyre load. The higher magnitude should not be interpreted as improved consistency: it indicates larger fluctuations, which may reduce the combined force capability of a load-sensitive tyre.
Set 6 provides the most consistent vertical load above 5 Hz, but it also produces the largest overshoot in sprung-mass displacement.
The complete-vehicle assessment must therefore balance chassis and aerodynamic-platform control against dynamic tyre-load variation [5,8,9].

4.5.2 Roll Response

A complementary reduced-order model was used to investigate the effect of the selected characteristics on roll dynamics. In this case, the damping forces generated by the four dampers were converted into an equivalent resisting roll moment using the suspension motion ratios. A secant roll damping coefficient was then evaluated at a reference roll velocity corresponding to a prescribed equivalent damper shaft velocity: [2,5]

$$c_{\phi,\mathrm{sec}} = \frac{|M_d(\dot{\phi}_{\mathrm{ref}})|}{|\dot{\phi}_{\mathrm{ref}}|}$$

where M_d is the total roll moment generated by the dampers. The corresponding critical value was calculated as

$$c_{\phi,\mathrm{cr}} = 2\sqrt{K_\phi I_\phi}$$

where K_ϕ is the total roll stiffness, including the contributions of the ride springs and anti-roll bars, and I_ϕ is the equivalent roll moment of inertia. The roll-based equivalent damping ratio was therefore defined as

$$\zeta_{\phi,\mathrm{eq}} = \frac{c_{\phi,\mathrm{sec}}}{c_{\phi,\mathrm{cr}}}$$

The anti-roll bars increase K_ϕ, and consequently the critical roll damping coefficient, without directly contributing to the dissipative roll moment.

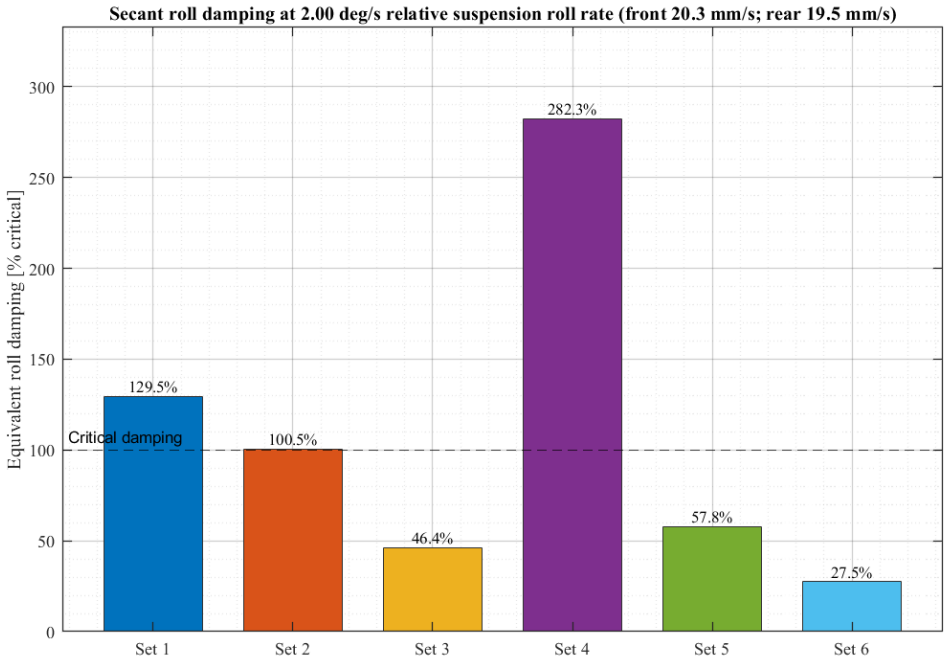


Figure 4.5 Equivalent roll damping ratio estimated from the secant damping coefficient

The same lateral-acceleration step was applied to every configuration. Figure 4.6 reports roll angle and contact-patch vertical loads. Roll angle describes sprung-mass platform control, while the left-to-right tyre-load difference describes the transient development of lateral load transfer. Figure 4.5 provides the corresponding secant-based roll damping comparison.

Since the dampers generate no force at zero suspension velocity, which means that no preload due to the gas pressure is considered, changing the damper characteristic does not modify the final steady-state roll angle or the final static load transfer when all stiffness parameters remain unchanged. The relevant differences are therefore found in

the rise time, overshoot, settling time and transient front-to-rear distribution of the vertical tyre loads.

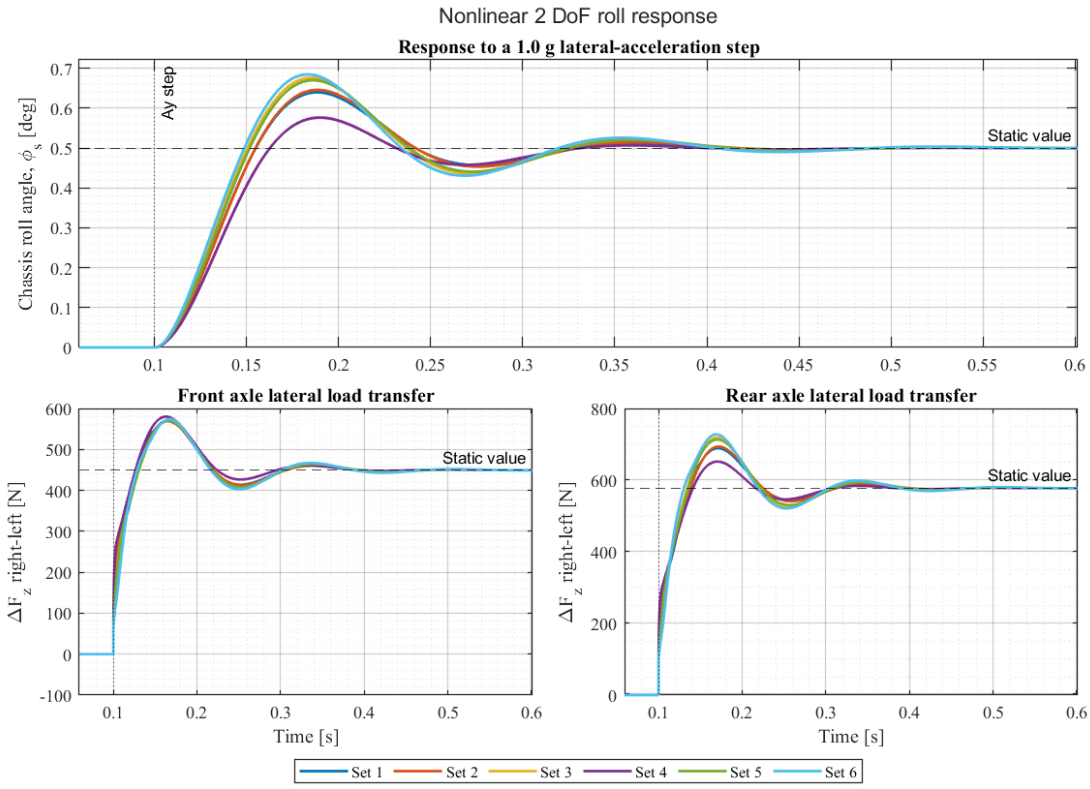


Figure 4.6 Nonlinear roll step response for the selected damper characteristics

Again, Figure 4.6 shows that Set 6 produces the largest overshoot, while Set 4 is the most heavily damped configuration, consistently with the calculated secant roll-damping ratios at the reference damper-shaft velocity and roll rate.

The role of these reduced-order analyses was to interpret the differences among the six selected curves and to identify the mechanisms through which the dampers affect platform control and contact-patch loading. The final assessment is performed in chapter 5 using the validated VI-CarRealTime model under representative manoeuvres. The comparison is based on wheel-lift occurrence, vertical tyre-load transients and handling-related quantities such as yaw rate, sideslip angle and steering input, together with their effect on the overall vehicle performance.

5 Damper Setup Tuning

5.1 Objectives and KPI Analysis

The objective of this chapter is to identify a damper setup that maximises the dynamic performance of the Formula Student prototype by exploiting the characteristics of the available passive hydraulic dampers. The tuning process is conducted after the previous validation based on experimental tests and within the constraints imposed by the existing suspension hardware and focuses on improving tyre grip, vehicle stability, and robustness under typical Formula Student driving conditions.
The goal is not to identify a single universally optimal configuration that is the best in every aspect, but to determine a damper setup that provides a favourable compromise between performance and controllability across a wide range of operating conditions. Damper optimisation changes the transient evolution of tyre loads rather than the total quasi-steady load transfer. Since longitudinal and lateral tyre forces depend on instantaneous vertical load, the comparison focuses on tyre-load histories together with yaw response, sideslip angle, wheel contact and lap time [2-8].
Based on these considerations, the most suitable setup is identified by comparing a limited number of representative damper configurations, previously identified in Chapter 4, using a set of vehicle-level performance and stability metrics derived from simulation results.

5.2 Simulation Setup and Evaluation Metrics

The damper configurations selected in Chapter 4 are implemented in the validated VI-CarRealTime model and evaluated through offline simulations using a virtual driver. All simulations are performed on the same reference track, representative of Formula Student Autocross and Endurance layouts and consistent with the circuit used during the on-track test sessions.
All vehicle parameters other than the damper force-velocity characteristic are kept constant. The same tyre model, suspension geometry, spring rates, mass distribution and powertrain assumptions are used in every case. The same damper curve is applied at all four corners.
The evaluation of the damper setups is based on a combination of performance-related and stability-related metrics. The primary metrics considered in this study are:

- Lap time around a test track, used as a global indicator of performance.
- Wheel-lift occurrence and duration, used as indicators of contact-patch consistency. These quantities are not interpreted as direct measures of total load transfer.
- Vertical tyre load behaviour, analysed through minimum values (near wheel-lift phenomena) and transient variations of F_z, to assess load variations and consistency.
- Yaw rate and vehicle sideslip angle β, used to evaluate handling balance and rotational behaviour.
- Steering input, considered as an indicator of driver workload and controllability, particularly in transient manoeuvres.

This set of metrics allows the comparison of damper setups not only in terms of peak performance, but also with respect to vehicle stability and robustness, key aspects especially in Endurance events.

5.3 Standardised Steering Chirp Manoeuvre for Damper Setup Evaluation

To discriminate further between sets with similar lap times and global handling metrics, a standardised steering chirp was introduced. The test provides a controlled open-loop excitation over a broad frequency range and supports a direct comparison of the vehicle response.

The manoeuvre consists of a continuous sinusoidal steering wheel input with increasing frequency (chirp), applied at a constant vehicle speed. The steering wheel angle is swept between ±45°, which is a typical steering wheel angle range for dynamic events, with the excitation frequency ranging from quasi-static conditions up to 4 Hz. The amplitude of the steering input is selected such that peak lateral accelerations approach 2 g, ensuring that the vehicle operates both in the linear and nonlinear regions of tyre lateral force generation, close to its full potential, as can occur during an Autocross event. Constant vehicle speed reduces variations associated with longitudinal demand and makes the lateral response easier to compare, although the tyre and suspension dynamics remain coupled.

This manoeuvre excites the main dynamic modes involved in cornering, including chassis roll motion, tyre transient response, and yaw dynamics. By varying only the damper force-velocity characteristics between simulations, the test enables a direct comparison of how different damping setups affect:

- lateral acceleration build-up and phase relative to steering input
- yaw rate response and rotational stability
- vehicle sideslip angle β and oscillatory behaviour
- vertical tyre load transients and wheel load distribution

Compared to lap time simulations, the proposed steering chirp test eliminates the influence of driver model adaptation and path-following strategies. As a result, it provides a more objective basis for evaluating the frequency-dependent effectiveness of different damper setups, particularly when multiple configurations produce similar performance in terms of lap time.

The steering wheel angle is used as the commanded input within the virtual driver interface, while the resulting vehicle response is assessed through measured lateral acceleration, yaw rate, sideslip angle, vertical wheel loads, and damper shaft velocities.

5.3.1 Frequency Response Function

The frequency-domain analysis used the 43 s steering chirp described above. Vehicle speed was held at approximately 60 km/h and the steering-wheel angle varied sinusoidally between ±45° with increasing frequency. The 0.5-4 Hz range was analysed for all six damper configurations under the same simulation conditions.

The signals were sampled at 100 Hz and de-meaned before spectral processing. No time-domain filter was applied. Empirical frequency-response estimates were calculated using a 512-sample Hann window, 75% overlap and a 4096-point FFT. Because the

input is a finite chirp and the vehicle response is nonlinear, these settings provide comparative estimates rather than formal linear time-invariant transfer functions.

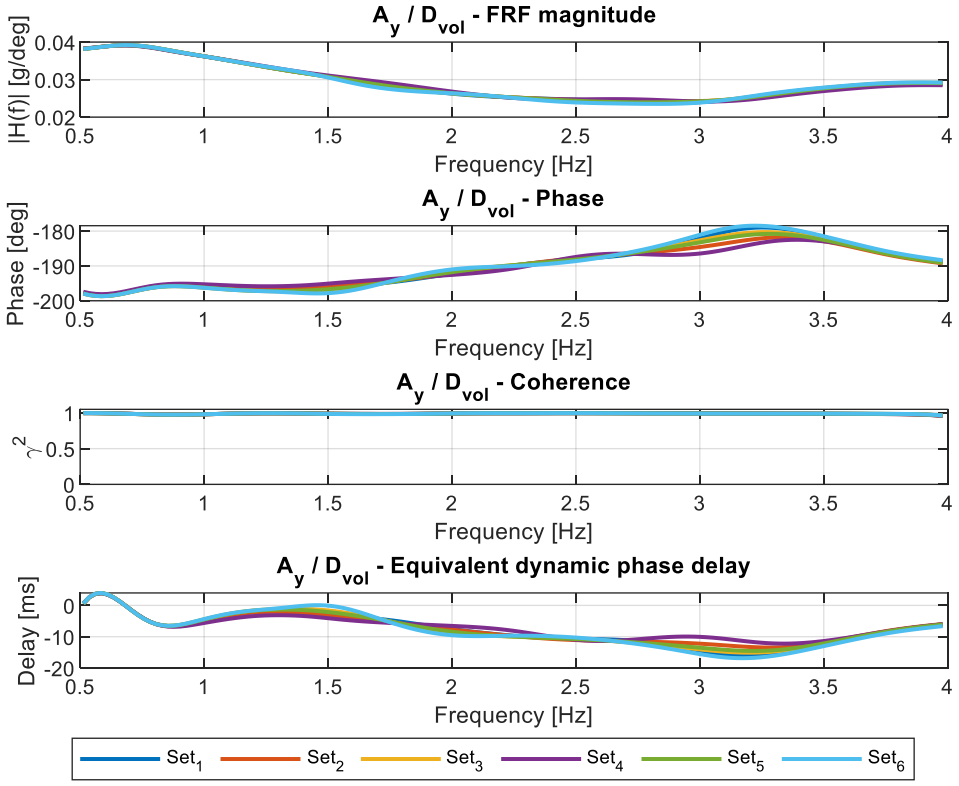


Figure 5.1 Empirical frequency-response estimate from steering-wheel angle to lateral acceleration

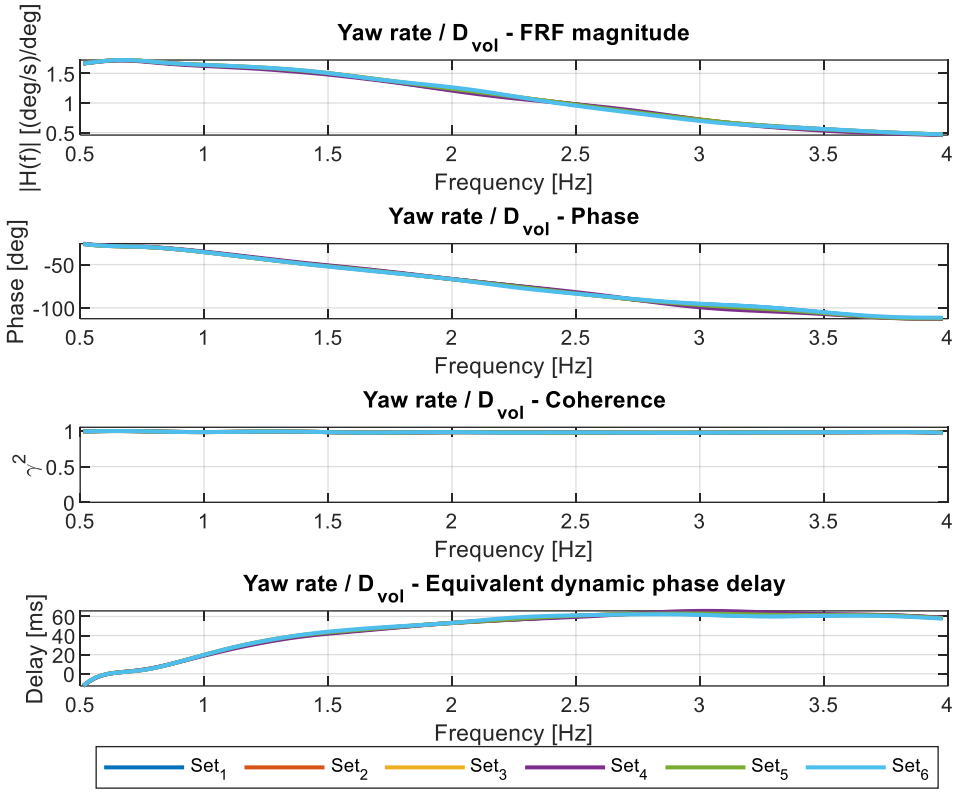


Figure 5.2 Empirical frequency-response estimate from steering-wheel angle to yaw rate

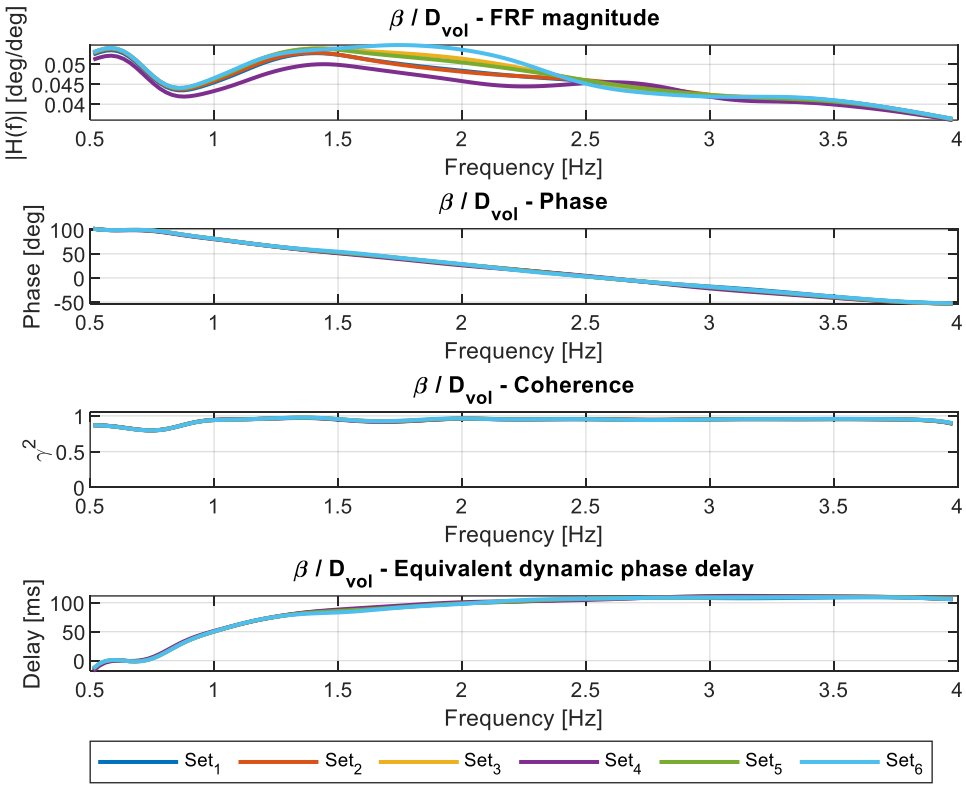


Figure 5.3 Empirical frequency-response estimate from steering-wheel angle to sideslip angle

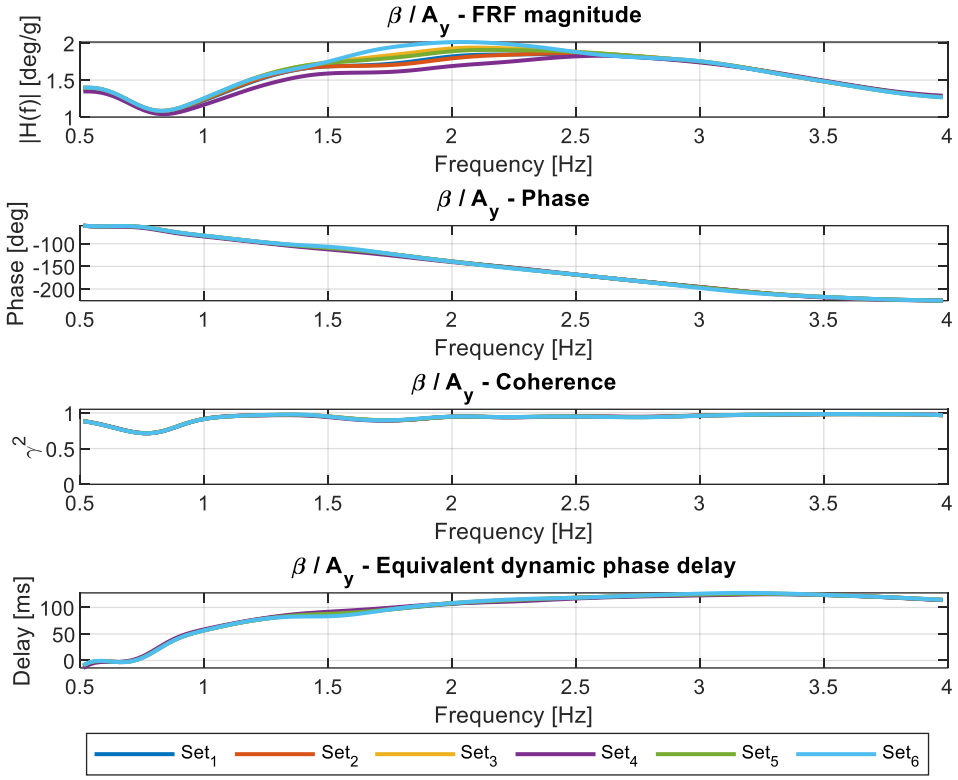


Figure 5.4 Empirical frequency-response estimate from lateral acceleration to sideslip angle

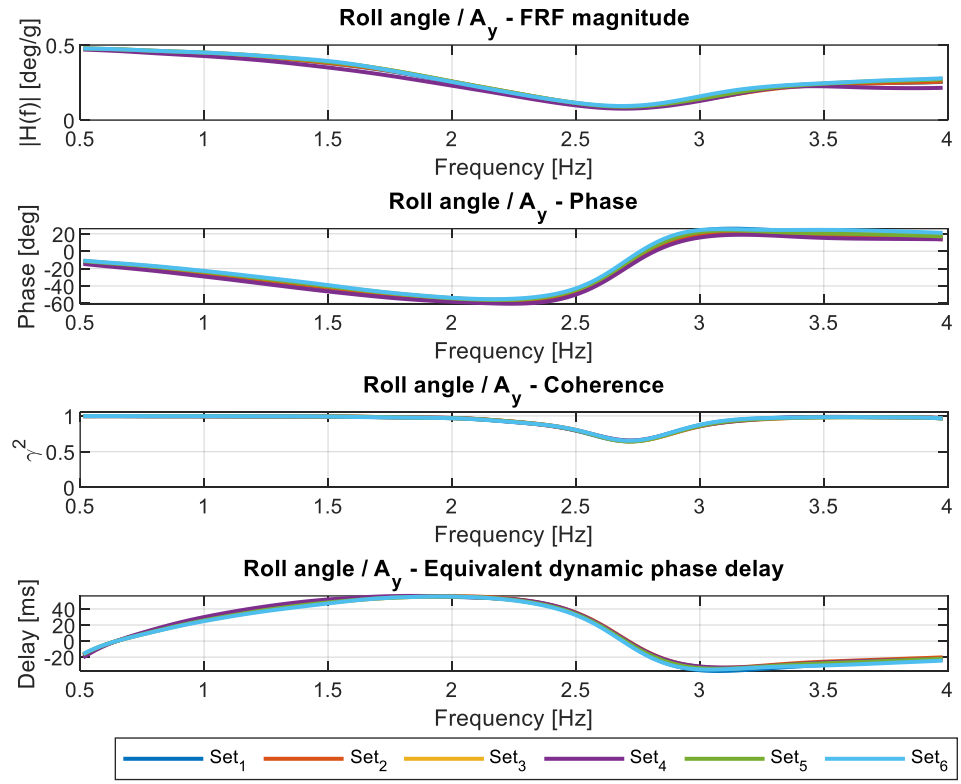


Figure 5.5 Empirical frequency-response estimate from lateral acceleration to roll angle

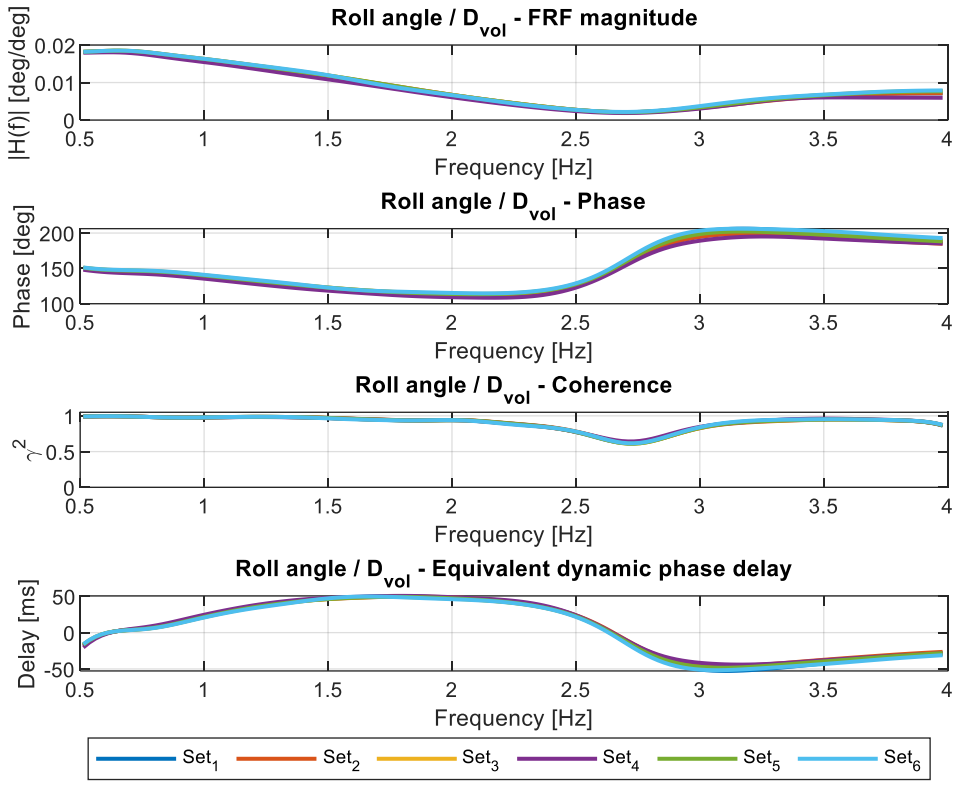


Figure 5.6 Empirical frequency-response estimate from steering-wheel angle to roll angle

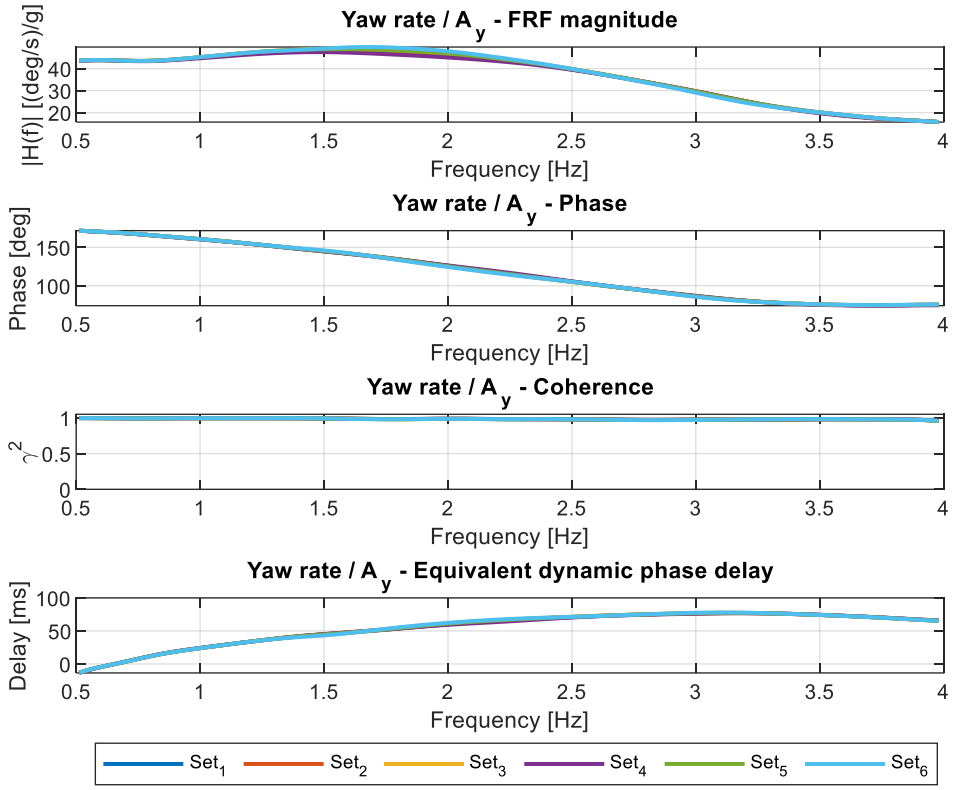


Figure 5.7 Empirical frequency-response estimate from lateral acceleration to yaw rate

For each pair of signals, the response convention was defined as

$$H(f) = \frac{Y(f)}{U(f)},$$

where U is the selected input signal and Y is the corresponding vehicle response. Steering-wheel angle was used as the input for the lateral-acceleration, yaw-rate, sideslip-angle, roll-angle and roll-rate responses. The ratios β/A_y, $Roll_Angle/A_y$ and $\text{Yaw Rate}/A_y$, instead, should be interpreted as relative frequency-response ratios between two vehicle outputs and not as causal input-output transfer functions.
The phase curves were unwrapped for representation. The equivalent dynamic phase delay was evaluated as

$$\tau_{\text{eq}}(f) = -\frac{\phi_{\text{dyn}}(f)}{2\pi f}.$$

Before calculating this quantity, the mean phase over the 0.5-0.8 Hz interval was removed. This correction prevents quasi-static phase offsets, including possible sign inversions between the considered channels, from being interpreted as physical time delays.
The steering amplitude produces lateral-acceleration peaks close to 2 g and therefore reaches the nonlinear operating region of the tyres. The curves in Figures 5.1-5.7 must be read as empirical estimates for one speed and steering amplitude excitation only.
The lateral-acceleration and yaw-rate estimates relative to steering-wheel angle show limited sensitivity to the damper set. The six magnitude curves largely overlap, while

coherence remains close to unity. The high coherence is expected for deterministic simulated signals and confirms numerical consistency.
Within this manoeuvre, damping changes do not substantially alter the main lateral-acceleration and yaw-rate gains.
A clearer separation appears in the sideslip response between approximately 1.3 and 2.5 Hz, as shown in Figure 5.3-5.4. Set 4 generally produces the lowest sideslip magnitude for both steering-wheel angle and lateral acceleration as reference signals, while Set 6 and some less-damped sets show larger responses.
Sideslip dynamics are therefore more sensitive to the selected characteristic than the main lateral-acceleration and yaw-rate gains. A lower sideslip magnitude alone does not demonstrate better handling: it must be considered with yaw response, tyre-load variation and lap time, since greater rear stability may also be associated with a slower, more understeering closed-loop response.
For a real driver, a more stable response may increase confidence, especially in Autocross, where track familiarisation is limited. This point cannot be demonstrated by the present virtual-driver analysis and requires subjective track assessment. The following sections therefore use only objective closed-loop indicators.

The roll-related responses provide a further distinction among the damper configurations, as shown in Figure 5.5 and 5.6. Set 4 generally exhibits the lowest roll-angle response, whereas Set 6 tends to produce higher magnitudes, especially in the intermediate- and high-frequency ranges. This result is consistent with the markedly different damping levels of the two configurations.
Overall, the frequency-domain analysis does not identify a unique optimal damper configuration. Its main contribution is to show that damper selection has a greater influence on sideslip and roll responses than on the global lateral-acceleration and yaw-rate gains. The final setup evaluation must therefore combine these results with virtual-driver lap time, vertical wheel-load behaviour and wheel-lift occurrence.

5.4 Comparison of Lap Time and Global Vehicle Behaviour

The six damper configurations were first compared through complete laps performed by the same virtual driver on the same track. All vehicle and simulation parameters other than the damper force-velocity characteristics were kept unchanged.
The virtual-driver parameters are identical in every run. The resulting steering, throttle and brake commands are not identical because the driver operates in closed loop and reacts to each simulated vehicle. Differences can therefore be attributed to the damper set within this specific driver-vehicle model.

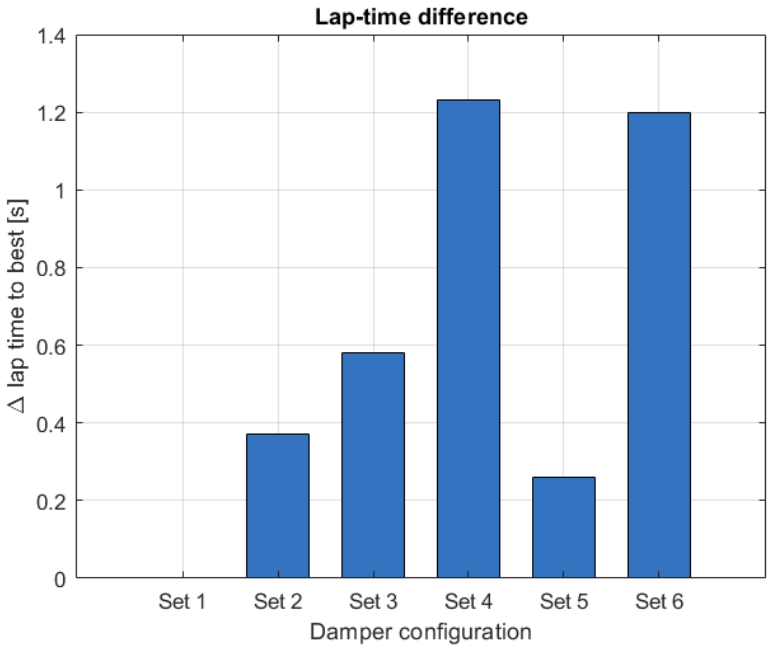


Figure 5.8 Lap-time variation relative to Set 1

As shown in Figure 5.8, Set 1 achieved the minimum lap time and is used as the reference. Set 5 and Set 2 followed with penalties of approximately 0.26 s and 0.37 s, while Set 3 was approximately 0.58 s slower. The largest penalties were obtained with Sets 6 and 4, both about 1.2 s behind Set 1.

This result is particularly relevant when related to the equivalent low-speed damping levels introduced in Chapter 4. Set 4 has the highest equivalent compression and rebound damping, whereas Set 6 is the least damped, particularly in rebound. These two extremes produced the largest lap-time penalties, while the best results came from the intermediate range. This does not establish a general optimum because the dampers are nonlinear and the equivalent values were used only for screening. It nevertheless agrees with the frequency-dependent compromise described for suspension damping in [5].

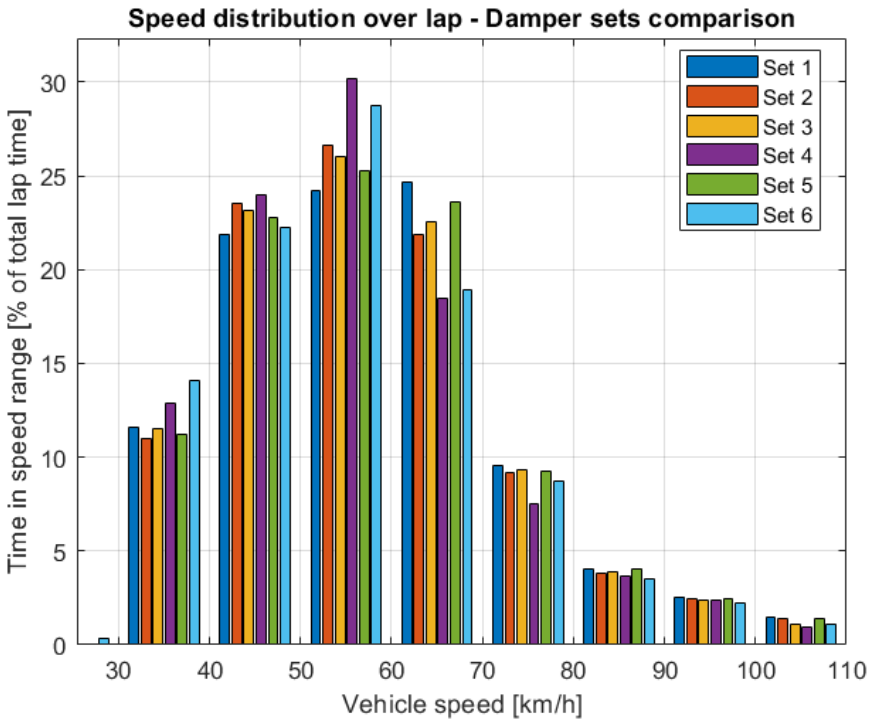


Figure 5.9 Vehicle-speed distribution over the simulated laps

The time-weighted vehicle-speed distributions in Figure 5.9 provide further insight into the lap-time differences. Most of the lap was completed between approximately 40 and 70 km/h for all configurations, confirming that the six simulations covered comparable operating conditions. Set 1 spent a larger fraction of the lap in the 60-70 km/h range, whereas Set 4 and Set 6 were more concentrated in the 50–60 km/h interval. This redistribution towards lower speed ranges is consistent with their larger lap-time penalties. Above approximately 80 km/h, the distributions become very similar because these ranges mainly correspond to the fastest and less handling-limited sections of the track, but a small prevalence of Set 1 and Set 5 can be seen.

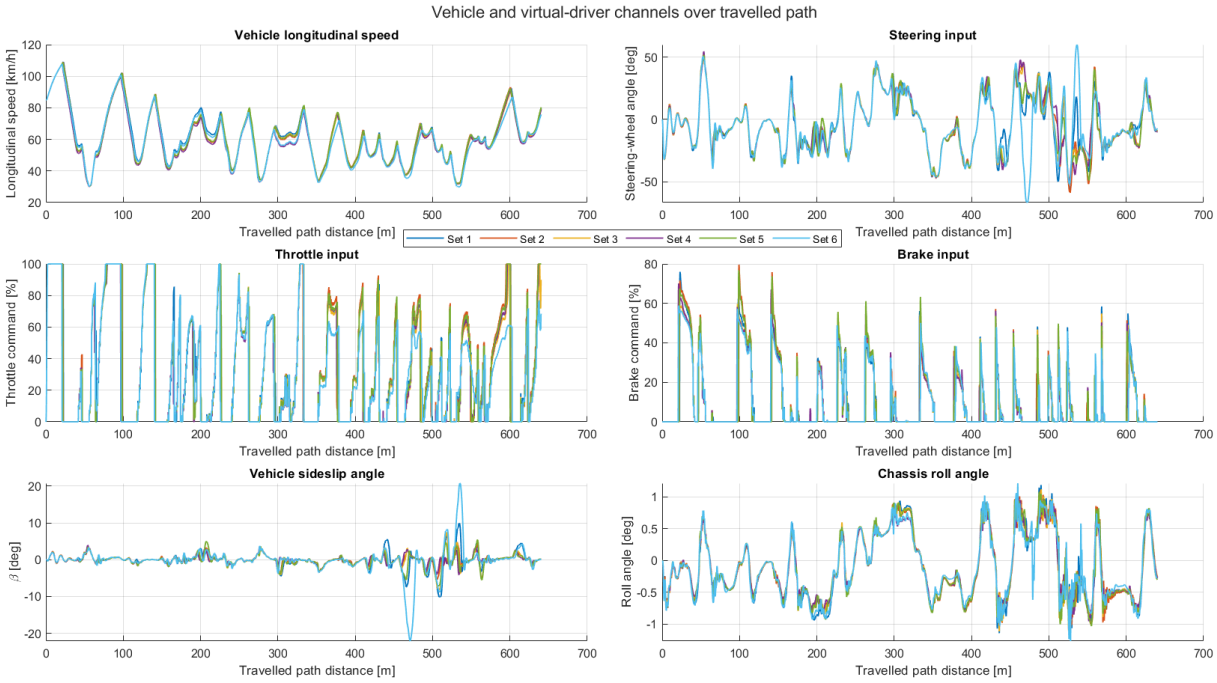


Figure 5.10 Spatial histories of steering-wheel angle, sideslip angle and vehicle path over the reference lap

The main vehicle states and virtual-driver commands are plotted against travelled distance in Figure 5.10. This representation associates differences with the same track sections despite the different lap times.
The speed, throttle, brake and roll-angle histories show a high degree of overlap over most of the lap. This confirms that the virtual driver completed a substantially equivalent driving task with each configuration. The chassis roll angle remains predominantly within approximately $\pm 1°$, and its overall trend changes only moderately between the sets. This is consistent with the fact that passive damping mainly modifies the transient development of suspension motion, while the quasi-steady roll response is primarily governed by springs and anti-roll bars.
The largest differences occur approximately between 450 and 550 m, where the steering input becomes more oscillatory and the sideslip response increases. Set 6 exhibits particularly large steering corrections and sideslip-angle excursions, with isolated values approaching $\pm 20°$. These excursions are also responsible for the markedly higher RMS sideslip value obtained for this configuration. Since Set 6 corresponds to the lowest equivalent damping level, its behaviour is consistent with insufficient control of the vehicle transient response.

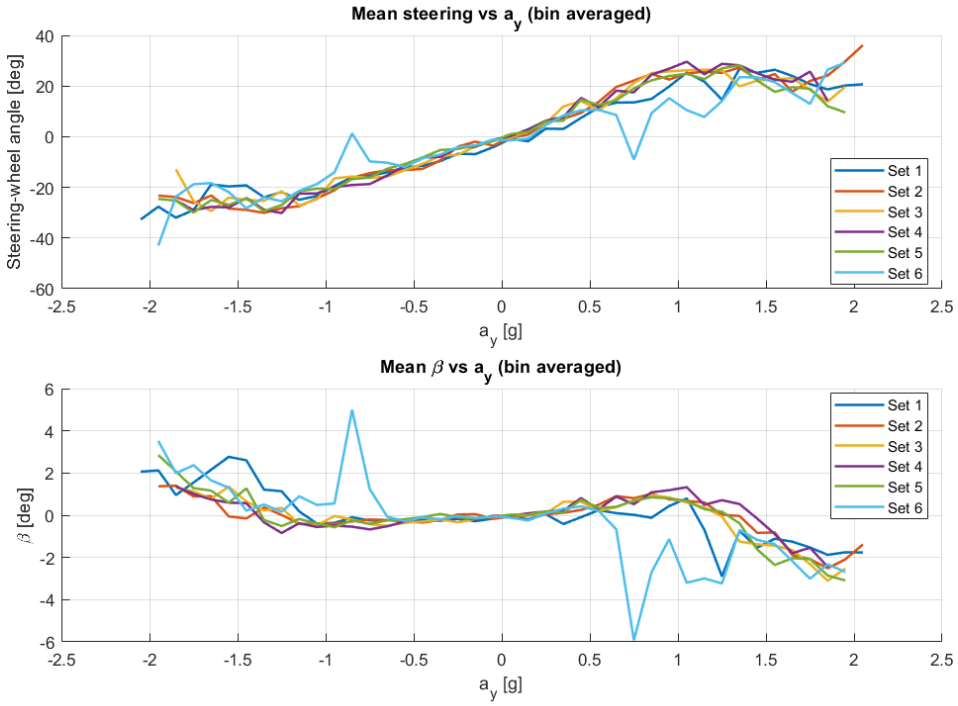


Figure 5.11 Bin-averaged steering-wheel angle and sideslip angle versus lateral acceleration

The bin-averaged steering and sideslip curves in Figure 5.11 confirm that Sets 1-5 produce broadly comparable macroscopic handling behaviour over the most frequently visited lateral-acceleration range. Around the central portion of the diagram, the steering-wheel angle increases approximately monotonically with lateral acceleration, while the mean sideslip angle remains relatively limited. Differences become more pronounced above approximately 1.2 g, where tyre nonlinearities and variations in vehicle speed increase the dispersion of the bin averages. These curves must be interpreted as descriptive full-lap relationships that also include nonlinear and highly dynamic behaviour, rather than as quasi-steady handling diagrams or measurements of the understeer gradient.

Set 6 again differs from the other configurations through abrupt variations in both steering angle and sideslip. These discontinuities are consistent with the spatial histories and indicate that its global RMS results are strongly influenced by a limited number of severe transient events.

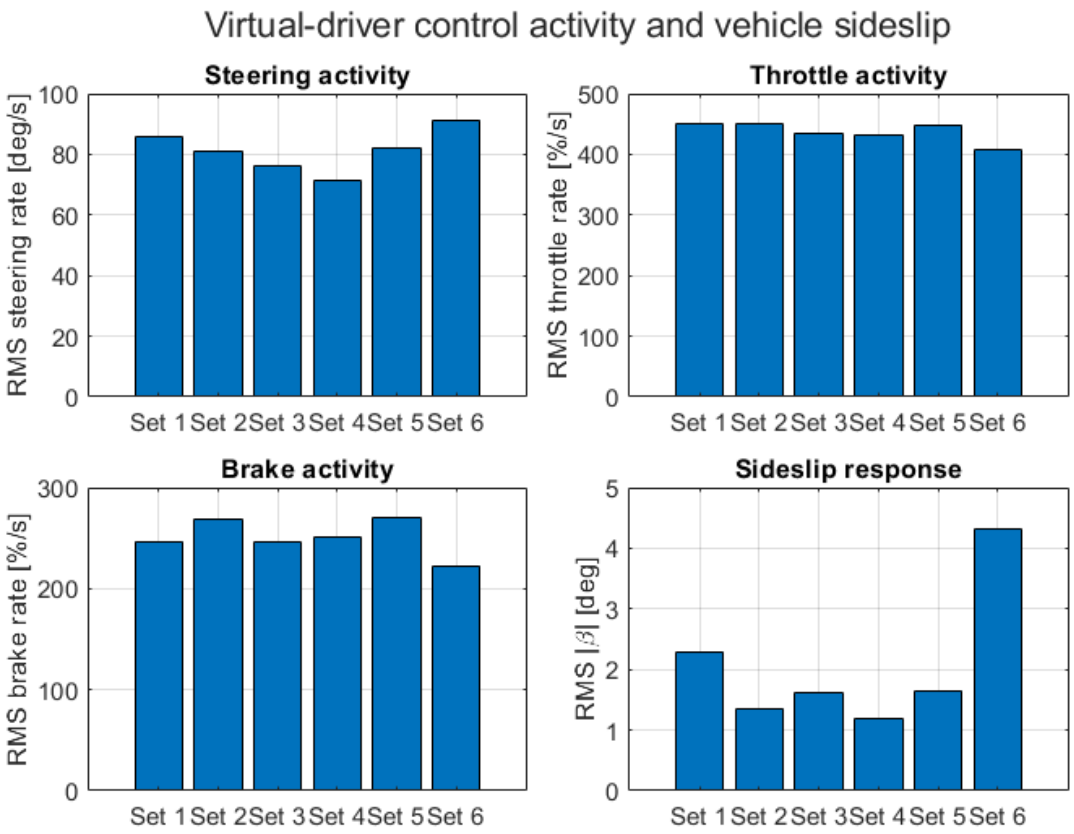


Figure 5.12 Virtual-driver command activity and sideslip-angle indicators

To quantify the activity required from the virtual driver, the RMS rates of the steering, throttle and brake commands were calculated. For a generic command $u(t)$, the adopted activity indicator can be expressed as

$$\dot{u}_{\mathrm{RMS}} = \sqrt{\frac{1}{T}\int_0^T \dot{u}^2\,(t)\,\mathrm{d}t}.$$

These quantities measure the rapidity of the simulated control actions and are reported in Figure 5.12. They are comparative indicators, not direct measurements of subjective driver workload.

Set 4 produced the lowest steering-rate RMS, approximately 72 deg/s, while Set 6 produced the highest value, approximately 92 deg/s. Sets 1, 2 and 5 occupied an intermediate range of approximately 82-86 deg/s. Set 6 simultaneously showed the lowest throttle- and brake-rate RMS values. This combination does not necessarily indicate easier vehicle control: together with its high sideslip response and lap-time penalty, it suggests that the virtual driver was forced to adopt a less aggressive driving style to adapt to the lack of control of the platform.

The RMS sideslip angle provides the clearest distinction between the configurations. Sets 2-5 remained approximately between 1.2° and 1.7°, while Set 1 reached approximately 2.3°. Set 6 exceeded 4°, mainly because of the large excursions previously identified. Set 4 achieved the lowest sideslip RMS and the lowest steering activity, but this was accompanied by the largest lap-time penalty, which means that the virtual driver was fighting a lot with understeering. Lower control activity must therefore not automatically be interpreted as superior drivability, since it may also result from a less responsive vehicle.

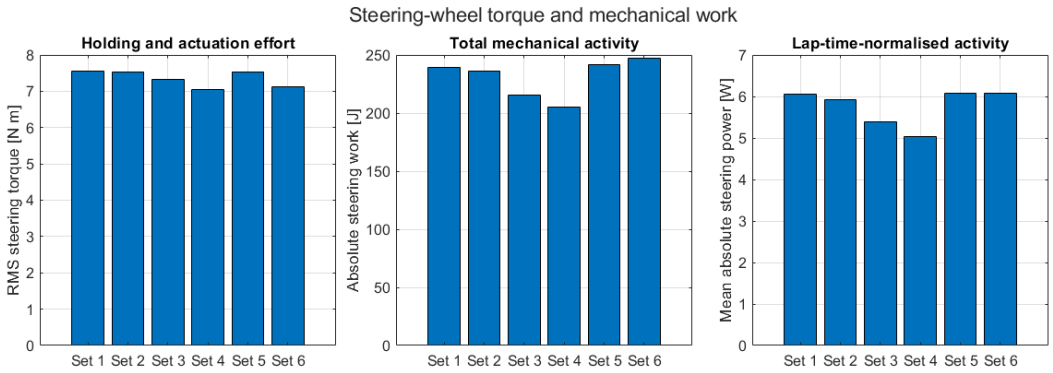


Figure 5.13 Steering-wheel torque and mechanical-work indicators

Steering effort was further evaluated using the steering-wheel torque channel. The RMS torque represents the combined holding and actuation effort, while the instantaneous mechanical power was calculated as

$$P_{\mathrm{sw}}(t) = M_{\mathrm{sw}}(t)\dot{\delta}_{\mathrm{sw}}(t).$$

Since positive and negative contributions can cancel over a complete lap, the principal integral indicator was the absolute mechanical work,

$$W_{\mathrm{sw,abs}} = \int_0^T |P_{\mathrm{sw}}(t)|\ \mathrm{d}t,$$

Together with mean absolute power, these quantities describe the mechanical activity exchanged at the steering-wheel coordinate; the results are shown in Figure 5.13. They do not represent electrical energy consumption or the metabolic effort of a real driver. The RMS steering torque varies relatively little between configurations. Larger differences are observed in absolute steering work. Set 4 requires the lowest value, approximately 290 J, followed by Set 3 at approximately 307 J. Set 6 reaches approximately 350 J despite its comparatively moderate torque RMS. Its high mechanical work is therefore mainly associated with the greater steering-wheel angular activity rather than with a higher holding torque. The mean absolute power leads to the same conclusion, with Set 4 at approximately 7.1 W and Sets 5 and 6 close to 8.6 W. Set 1 provides the best outright performance, while Set 5 initially appears to be a relevant compromise candidate. Its lap-time penalty is about 0.26 s and its sideslip response is lower than that of Set 1, without the severe excursions of Set 6. The wheel-lift duration results in the next section are needed before making the final selection.

5.5 Wheel Load Management and Wheel Lift Analysis

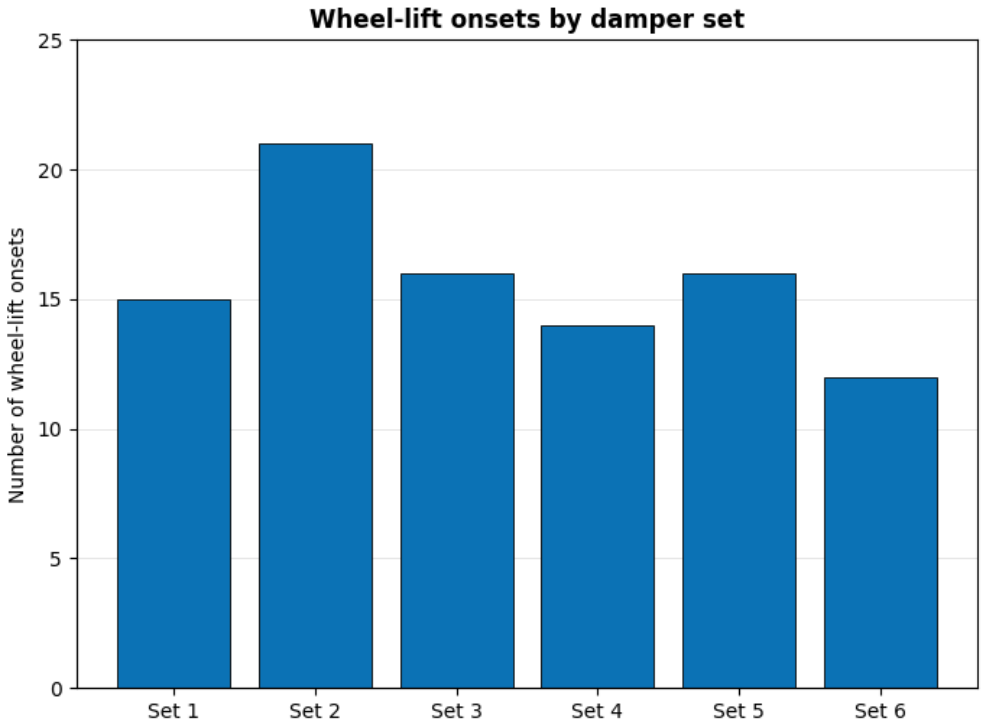


Figure 5.14 Number of wheel-lift onsets for each damper set

The total transition count is reported in Figure 5.14. Set 2 produced the highest number, with 21 wheel-lift onsets. Sets 3 and 5 produced 16 events, Set 1 produced 15 and Set 4 produced 14. The minimum count was obtained with Set 6, with 12 events.
This ranking cannot be considered independently from the performance results. Set 6 achieved the lowest event count but also showed one of the largest lap-time penalties, the highest RMS sideslip angle and the most severe rear end grip loss events. Similarly, the relatively low count obtained with Set 4 was accompanied by the slowest lap. A reduction in event count may therefore result partly from lower local speed or lower lateral demand rather than exclusively from improved wheel-load control.

Table 5.1 Wheel-lift count and duration metrics for the six damper sets

Damper set	Lap time [s]	Front events	Rear events	Total events	Cumulative wheel-lift time [s]	Maximum event duration [s]
Set 1	39.52	2	13	15	1.36	0.18
Set 2	39.89	5	16	21	1.54	0.17
Set 3	40.10	3	13	16	1.32	0.16
Set 4	40.75	0	14	14	1.27	0.17
Set 5	39.78	0	16	16	1.60	0.19
Set 6	40.72	0	12	12	1.30	0.19

Conversely, Set 1 combined the fastest lap with an intermediate number of contact-loss events. Set 5 was only approximately 0.26 s slower and produced one additional event. These two configurations consequently remain the most relevant candidates when performance and wheel-contact behaviour are considered together. The comparison should be completed using the event-duration quantities reported in Table 5.1, because a

setup producing several extremely short detachments may be preferable to one producing fewer but substantially longer losses of contact, but as shown in the last column of Table 5.1, the event duration is very short and very similar for all the configurations analysed.

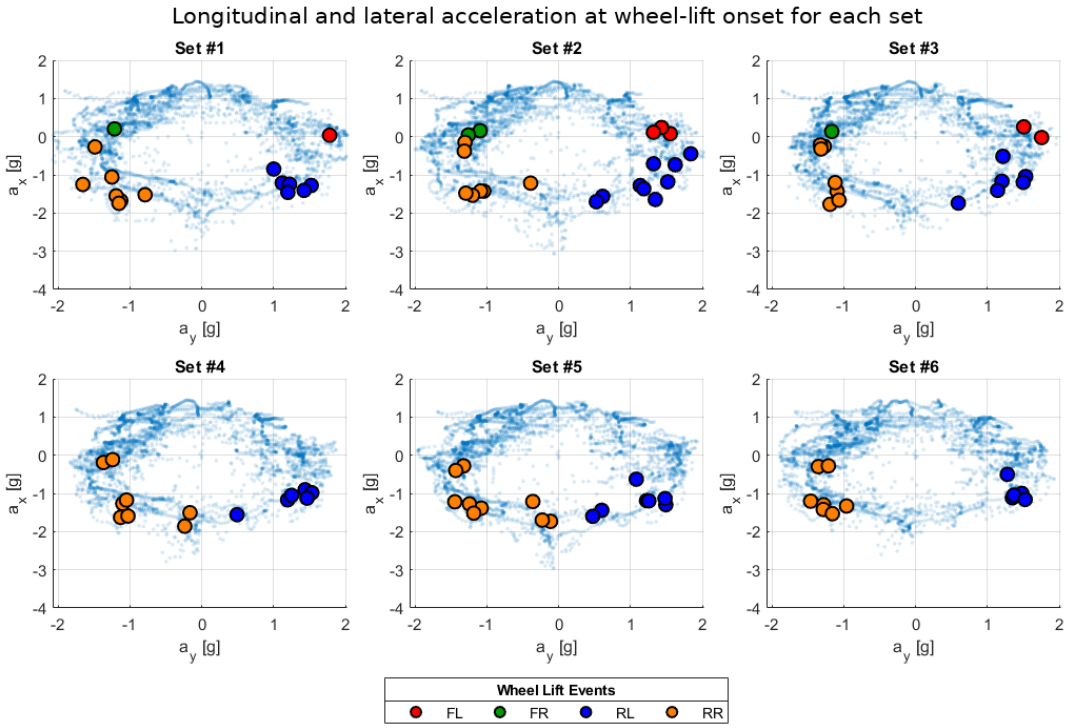


Figure 5.15 Longitudinal and lateral acceleration at wheel-lift onset

Figure 5.15 shows the longitudinal and lateral acceleration conditions at the onset of each event. With the adopted sign convention, positive lateral acceleration is predominantly associated with lift of the left-side wheels, while negative lateral acceleration is associated with lift of the right-side wheels. This is consistent with loss of contact occurring at the unloaded wheels on the inside of the turn.

A clear difference can also be observed between the front and rear axles. Front-wheel lift markers appear only for Sets 1-3 and are concentrated close to zero longitudinal acceleration, at relatively high absolute lateral acceleration. Rear-wheel lift is instead present in all six configurations, and most events occur during combined cornering and braking, with negative longitudinal acceleration frequently exceeding 1 g in magnitude. Braking transfers vertical load towards the front axle and further unloads the rear axle; when combined with lateral load transfer, this condition makes the inside rear wheel particularly susceptible to loss of contact.

The interpretation is consistent with tyre load sensitivity and with the longitudinal and lateral load-transfer mechanisms described in [2-4]. Suspension jacking is a plausible contribution because forces transmitted through the suspension geometry can generate vertical components. The present scatter plots do not isolate it from elastic load transfer, aerodynamic loading, road excitation and damper transients, so it is not treated as a demonstrated cause.

The absence of front-wheel lift in Sets 4-5-6 suggests that the change in damper characteristics modified the transient distribution of wheel loads between the two axles. However, all three configurations still produced repeated rear-wheel detachments. The

result therefore does not indicate the elimination of wheel lift, but rather a concentration of the phenomenon at the rear axle and during combined braking and cornering. Event count alone would favour Set 6, but its poor sideslip behaviour and lap-time result show why that metric is insufficient. Set 2 represents the opposite case, with a competitive lap and limited RMS sideslip but the largest number of contact-loss transitions. Set 1 combines the best performance with an intermediate count. Set 5 remains competitive in lap time.

6 Conclusions

This thesis investigated the influence of passive hydraulic damper characteristics on the dynamic behaviour of the SC24 Formula Student prototype, with the objective of identifying an effective baseline configuration without modifying the existing suspension hardware. The work combined vehicle dynamics theory, experimental damper data, on-track telemetry, post-processing tools for data analysis and vehicle-level simulation, providing a structured alternative to a purely trial-and-error setup process.

A physics-based vehicle model implemented in VI-CarRealTime was first assessed against experimental data collected during steering-frequency sweeps, double lane changes and slalom manoeuvres. The comparison included lateral and longitudinal acceleration, yaw rate, vehicle sideslip angle, wheel rotational speeds and vehicle speed. Although a perfect point-by-point correspondence was neither expected nor achieved, the model reproduced the main amplitudes, trends and transient responses observed on the real vehicle. The resulting correlation was considered adequate for the primary purpose of the work, namely the comparative evaluation of damper configurations under consistent operating conditions.

The experimental damper force-velocity characteristics supplied by Lorandi Sospensioni were subsequently processed and implemented directly in the virtual model. Because an exhaustive exploration of all low-speed and high-speed compression and rebound adjustments would have been impractical, an equivalent low-speed damping ratio was calculated at a reference shaft velocity of 20 mm/s. This parameter was used only as a preliminary screening indicator, rather than as a complete description of the nonlinear damper behaviour. Six representative force-velocity characteristics were retained and applied identically to all four corners of the vehicle, allowing the effect of the damper curve to be isolated from additional front-to-rear setup variables.

A standardised 43 s steering chirp was introduced to complement the full-lap analysis with a controlled and repeatable excitation. The manoeuvre was performed at approximately 60 km/h, with a steering-wheel amplitude of ±45° and an excitation range extending to 4 Hz. The resulting frequency-response functions provided a direct comparison of the lateral, yaw, sideslip, roll and wheel-load responses generated by the six damper characteristics. This analysis was particularly useful because damper tuning primarily influences transient and frequency-dependent behaviour, which cannot be fully represented by lap time or other single-value performance indicators.

The complete-lap simulations showed that the damper characteristic had a measurable influence on vehicle performance. Set 1 achieved the fastest lap, with a time of 39.520 s. Set 5 and Set 2 followed with penalties of 0.26 s and 0.37 s, corresponding respectively to 0.66% and 0.94%. Set 3 was 0.58 s slower, while the two configurations representing the most extreme damping levels produced the largest penalties: Set 4 was 1.23 s slower and Set 6 was 1.20 s slower, corresponding to approximately 3.1% and 3.0%.

These results indicate that neither the highest nor the lowest damping level provided the best global performance. The highest-damped configuration reduced several indicators of steering and sideslip activity but resulted in the slowest lap, suggesting a less responsive overall vehicle behaviour. Conversely, the least-damped configuration produced the highest steering-rate RMS and a sideslip RMS of 4.32°, with individual sideslip excursions exceeding 22° in absolute value. This behaviour indicates

insufficient control of the most severe transient responses, despite the relatively low number of wheel-lift events.

The virtual-driver metrics further demonstrated that controllability cannot be assessed through a single parameter. Steering-wheel torque RMS remained within a relatively narrow range for all configurations, while greater differences were observed in steering rate and absolute mechanical work. Set 6 produced the highest absolute steering work, equal to approximately 351 J, because its large and rapid steering corrections compensated for its comparatively moderate torque level. Set 4 required the lowest steering activity and mechanical work but did not convert this reduction into improved lap performance. Consequently, lower driver-control activity does not necessarily indicate a better setup, since it may also be associated with a vehicle that cannot sustain the same pace. Nevertheless, it remains a useful indicator, especially during the Endurance event, where high summer temperatures and prolonged driving place substantial physical demands on the drivers.

Wheel-contact analysis provided an additional criterion for discriminating between configurations. Wheel lift occurred predominantly at the rear axle during combined braking and cornering, when longitudinal load transfer further unloaded the inside rear wheel and added to the lateral load transfer. Suspension jacking may also have contributed, but the present analysis did not isolate it from the other mechanisms. The short front-wheel events detected in Sets 1-3 lasted between 0.01 and 0.04 s, whereas the longest rear-wheel events ranged between 0.13 and 0.19 s.

Set 2 produced the largest number of contact-loss transitions, with 21 events, while Set 6 produced the minimum, with 12. However, the duration-based metrics led to a more meaningful interpretation. Set 4 and Set 6 recorded the shortest total wheel-lift times, respectively 1.27 s and 1.30 s, but both were associated with lap-time penalties of approximately 3%. Set 5 produced the longest total wheel-lift duration, equal to 1.60 s or 4.02% of the lap. Set 1 instead combined the fastest lap with 15 events, a total wheel-lift duration of 1.36 s and a maximum individual duration of 0.18 s.

No configuration minimised every performance, stability and wheel-contact indicator. Set 1 achieved the fastest lap and a shorter cumulative wheel-lift duration, whereas Set 5 produced the longest cumulative wheel-lift duration of the six sets. However, Set 5 was only 0.26 s slower, corresponding to 0.66%, and its maximum individual wheel-lift duration was practically equal to that of Set 1. It also produced no front-wheel-lift events, maintained an intermediate steering-rate demand and showed a lower RMS sideslip response than Set 1. In addition, the reduced-order analysis indicated a more favourable high-frequency contact-patch load response for Set 5. Set 5 therefore provides the most favourable overall compromise in the investigated dataset. It should be regarded as the most effective baseline for subsequent track testing, not as a universal or globally optimal setup.

Several limitations must be considered when interpreting these results. The available dynamometer data consisted of static force-velocity curves and did not separately identify hysteresis, internal friction, temperature dependence or frequency-dependent damper behaviour. The same characteristic was applied at all four corners, preventing the investigation of independent front-to-rear tuning. The tyre model and braking-system representation also introduced uncertainties, particularly during combined braking and cornering and under the relatively low tyre temperatures encountered during the experimental tests.

The virtual-driver control metrics represent objective indicators of command activity and mechanical steering work, but they cannot reproduce subjective driver confidence, steering feel or physical workload.

An important future development would be to investigate the suspension geometry in greater depth and identify ways to increase the available travel, especially in extension. This could be achieved by modifying the rocker geometry to change the coilover installation ratio, together with the spring stiffness required to preserve the suspension vertical and roll rates, or by changing the clearance or length of the rebound stop located inside the damper.
This analysis could be extended to independent front- and rear-axle characteristics and to a wider combination of compression and rebound settings. Repeating the simulations and experimental tests on different track layouts and road-roughness conditions would finally allow the robustness of the selected setup to be assessed over the complete range of Formula Student Autocross and Endurance operating conditions.
Overall, the work demonstrates that a validated virtual vehicle model can provide an effective tool for reducing the number of damper configurations requiring physical testing and for identifying the dynamic mechanisms behind apparently similar lap-time results. Simulation does not replace track validation, but it can guide the setup process towards physically meaningful candidates, reducing development time and improving the quality of subsequent experimental decisions.

Bibliography

[1] Formula Student Germany, Formula Student Rules 2026, version 1.1, 2025.

[2] M. Guiggiani, The Science of Vehicle Dynamics: Handling, Braking, and Ride of Road and Race Cars, 2nd ed., Springer, Cham, 2018. doi: 10.1007/978-3-319-73220-6.

[3] C. Rouelle, 'The No Way Transfer, Part 1: Righting the Wrongs about Load Transfer,' Racecar Engineering, August 2021, pp. 54-56.

[4] C. Rouelle, 'The No Way Transfer, Part 2: The Difference between Suspended-Mass Geometric and Elastic Load Transfer, and the Influence of Kinematics,' Racecar Engineering, September 2021, pp. 50-53.

[5] A. Goodarzi and A. Khajepour, Vehicle Suspension System Technology and Design, Morgan & Claypool, 2017. doi: 10.2200/S00767ED1V01Y201704MEC002.

[6] S. P. Gacka and C. G. Doherty, 'Design Analysis and Testing of Dampers for a Formula SAE Race Car,' SAE Technical Paper 2006-01-3641, 2006. doi: 10.4271/2006-01-3641.

[7] S. Sahoo, E. P. De Reuben, D. Bakshi, H. Krishnan and A. Singh, 'Variation in Automotive Shock Absorber Damping Characteristics and Their Effects on Ride Comfort Attribute and Vehicle Yaw Response,' SAE Technical Paper 2021-26-0081, 2021. doi: 10.4271/2021-26-0081.

[8] B. Lacroix, P. Seers and Z. Liu, 'A Passive Nonlinear Damping Design for a Road Race Car Application,' SAE Technical Paper 2006-01-1984, 2006. doi: 10.4271/2006-01-1984.

[9] Y. Chen, X. Jing and L. Cheng, 'Frequency Domain Analysis and Design of Nonlinear Vehicle Suspension Systems,' in Handbook of Vehicle Suspension Control Systems, H. Liu, H. Gao and P. Li, Eds., IET, 2013, pp. 357-399. doi: 10.1049/PBCE092E_ch13.

[10] H. Kowalczyk, 'Damper Tuning with the Use of a Seven Post Shaker Rig,' SAE Technical Paper 2002-01-0804, 2002. doi: 10.4271/2002-01-0804.

[11] N. Moshchuk, C. Namuduri, F. Nardi, J. Ryu, R. Knoll and W. Golpe, 'A Passive Progressive Damping Design for Ride and Handling,' Proceedings of ASME IMECE2013, paper IMECE2013-64447, 2013. doi: 10.1115/IMECE2013-64447.

[12] J. C. Romero and S. E. Diaz, 'Design, Construction and Testing of a Shock Absorber Prototype for a Formula SAE Vehicle,' SAE Technical Paper 2006-01-3640, 2006. doi: 10.4271/2006-01-3640.

[13] J. L. L. Berretta and G. C. da Silva, 'FSAE Suspension Development in Virtual Environment,' SAE Technical Paper 2018-36-0231, 2018. doi: 10.4271/2018-36-0231.

[14] VI-grade, VI-CarRealTime 2024.2 and VI-SuspensionGen, vehicle dynamics and suspension modelling software, 2024.

[15] dSPACE, MicroAutoBox II Hardware Reference: Data Sheet MicroAutoBox II 1401/1511, revision May 2023.

[16] SBG Systems, Ellipse-N Miniature RTK Inertial Navigation System, product documentation.

[17] RLS, RM08 Miniature Rotary Magnetic Encoder, data sheet RM08D01, issue 18, 2026.

[18] Öhlins Racing AB, Shock Absorber for Formula Student and Formula SAE - TTX 25 Workshop Manual, 2013, and TTX25 MkII FSAE technical information.

[19] Kistler Instrumente AG, Non-contact optical sensors CORREVIT S-Motion Standard, Type 2055A, product documentation.